Check for updates

# Overexpression of stress granule protein TZF1 enhances salt stress tolerance by targeting *ACA11* mRNA for degradation in Arabidopsis

Siou-Luan He[1,2,3†], Bin Li[4,5†], Walter J. Zahurancik[3,6], Henry C. Arthur[3,6], Vaishnavi Sidharthan[3,6], Venkat Gopalan[3,6], Lei Wang[4,5*] and Jyan-Chyun Jang[1,2,3*]

[1]Department of Horticulture and Crop Science, The Ohio State University, Columbus, OH, United States, [2]Center for Applied Plant Sciences, The Ohio State University, Columbus, OH, United States, [3]Center for RNA Biology, The Ohio State University, Columbus, OH, United States, [4]Key Laboratory of Plant Molecular Physiology, Institute of Botany, Chinese Academy of Sciences, and University of Chinese Academy of Sciences, Beijing, China, [5]Academician Workstation of Agricultural High-Tech Industrial Area of the Yellow River Delta, National Center of Technology Innovation for Comprehensive Utilization of Saline-Alkali Land, Shandong, China, [6]Department of Chemistry and Biochemistry, The Ohio State University, Columbus, OH, United States

Tandem CCCH zinc finger (TZF) proteins play diverse roles in plant growth and stress response. Although as many as 11 TZF proteins have been identified in *Arabidopsis*, little is known about the mechanism by which TZF proteins select and regulate the target mRNAs. Here, we report that *Arabidopsis* TZF1 is a bona-fide stress granule protein. Ectopic expression of *TZF1* (*TZF1 OE*), but not an mRNA binding-defective mutant (*TZF1^{H186Y} OE*), enhances salt stress tolerance in *Arabidopsis*. RNA-seq analyses of NaCl-treated plants revealed that the down-regulated genes in *TZF1 OE* plants are enriched for functions in salt and oxidative stress responses. Because many of these down-regulated mRNAs contain AU- and/or U-rich elements (AREs and/or UREs) in their 3'-UTRs, we hypothesized that TZF1—ARE/URE interaction might contribute to the observed gene expression changes. Results from RNA immunoprecipitation-quantitative PCR analysis, gel-shift, and mRNA half-life assays indicate that TZF1 binds and triggers degradation of the *autoinhibited Ca^{2+}-ATPase 11* (*ACA11*) mRNA, which encodes a tonoplast-localized calcium pump that extrudes calcium and dampens signal transduction pathways necessary for salt stress tolerance. Furthermore, this salt stress-tolerance phenotype was recapitulated in *aca11* null mutants. Collectively, our findings demonstrate that TZF1 binds and initiates degradation of specific mRNAs to enhance salt stress tolerance.

KEYWORDS

stress granules, salt stress, ARE element, RNA decay, protein-RNA interaction, tandem CCCH zinc finger protein

## Introduction

Salinity stress is harmful to most non-halophyte plants, seriously limiting crop growth and productivity (Zhao et al., 2021). Plants have developed sophisticated mechanisms to temporarily adapt to high salt environments by altering gene expression, physiology, and metabolism (Zhu, 2002; Deinlein et al., 2014; Julkowska and Testerink, 2015; Zhu, 2016). Thus, unraveling the genetic mechanisms underlying salt stress tolerance could provide important clues to improve crop fitness and yields under prolonged salinity stress or in the regions with high soil salinity.

*Arabidopsis* tandem CCCH zinc finger (AtTZF) proteins play a key role in regulating various plant hormone-mediated growth and environmental responses. There are 11 *TZF* genes in *Arabidopsis* that are differentially expressed temporally and spatially (Jang, 2016). In the *AtTZF* gene family (hereafter as *TZF*), *TZF1* is ubiquitously expressed at a high level and the best characterized family member. TZF1 is a positive regulator of abscisic acid (ABA), sugar, and salt stress tolerance responses, while serving as a negative regulator of gibberellin (GA) responses (Lin et al., 2011; Han et al., 2014). In rice, OsTZF1, a homolog of *TZF1*, is involved in seed germination, seedling growth, leaf senescence, and oxidative stress tolerance (Jan et al., 2013). TZF2 and TZF3 act as positive regulators for ABA, oxidative, and salt stress responses, and as negative regulators for stress hormone methyl jasmonate (MeJA)-induced senescence (Huang et al., 2011, 2012; Lee et al., 2012). Furthermore, rice OsTZF2 (OsDOS), the homolog of TZF2, can delay MeJA-induced leaf senescence (Kong et al., 2006). TZF4/5/6 are positive regulators of ABA responses, while acting as negative regulators for GA and phytochrome-mediated seed germination responses (Kim et al., 2008; Bogamuwa and Jang, 2013). TZF7 to TZF 11 are positive regulators of vegetative growth and abiotic and biotic stress tolerance responses, and function as negative regulators for stress-induced transition to flowering (Sun et al., 2007; Blanvillain et al., 2011; Maldonado-Bonilla et al., 2014; Kong et al., 2021). Although TZF1/2/3/10/11 proteins have been shown to be redundantly involved in salt stress responses (Jang, 2016), the molecular mechanisms by which TZF proteins target mRNAs to govern the salinity stress response are still unclear.

Ribonucleoprotein (RNP) granules are membrane-less biomolecular condensates that generally form via liquid-liquid phase separation mediated by multivalent protein-protein, protein-RNA, and RNA-RNA interactions. The scaffold proteins in the RNP granules are characterized by having intrinsically disordered, low-complexity, or prion-like domains (Ripin and Parker, 2023; Solis-Miranda et al., 2023). Two of the best characterized cytoplasmic RNP granules are processing bodies (PBs) and stress granules (SGs), which are dynamically assembled in response to environmental stresses (Jang et al., 2020). Human tristetraprolin (hTTP), a prototypical TZF protein, controls mRNA stability by selective binding to target genes (Carballo et al., 1998). hTTP often binds AU-rich elements (AREs) in the 3'-UTR of mRNA and recruits target mRNAs to PBs and SGs for gene silencing through RNA decay and translational repression (Lai et al., 1999). In *Arabidopsis*, TZF1 was found to traffic between

cytoplasmic foci and nuclei and was colocalized with PB (DCP2) and SG (PABP8) markers (Pomeranz et al., 2010). TZF1 also binds polyU (Pomeranz et al., 2010) and ARE (Qu et al., 2014) specifically. Furthermore, TZF1 directly binds 3'-UTR of *Target of Rapamycin* (*TOR*) mRNA using its tandem zinc finger motif to affect *TOR* mRNA stability. The interaction of TZF1-*TOR* mRNA is necessary for root meristem cell proliferation by integrating both transcriptional and post-transcriptional regulation of gene expression (Li et al., 2019). Although the molecular mechanisms of hTTP in promoting mRNA degradation in animals has been characterized in great detail (Brooks and Blackshear, 2013), the mechanisms by which plant TZF proteins bind and elicit degradation of target mRNAs are poorly understood.

Plant TZF proteins play critical roles in salt, drought, oxidative, and many other stress responses, but the link between TZF-mediated stress tolerance responses and mRNA degradation has not been well-established. To date, it remains a challenge to unbiasedly identify genome-wide TZF target mRNAs and specific binding sites *in vivo*. Here, we show that TZF1 could enhance salt stress tolerance by binding to and initiating degradation of mRNAs encoding salt- or oxidative-stress responsive genes. As proof of principle, we performed detailed biochemical and molecular analyses to demonstrate that TZF1 enhances salt stress tolerance by binding to a specific 3'-UTR region of a down-regulated target gene *ACA11*, a negative regulator in salt stress signaling.

## Results

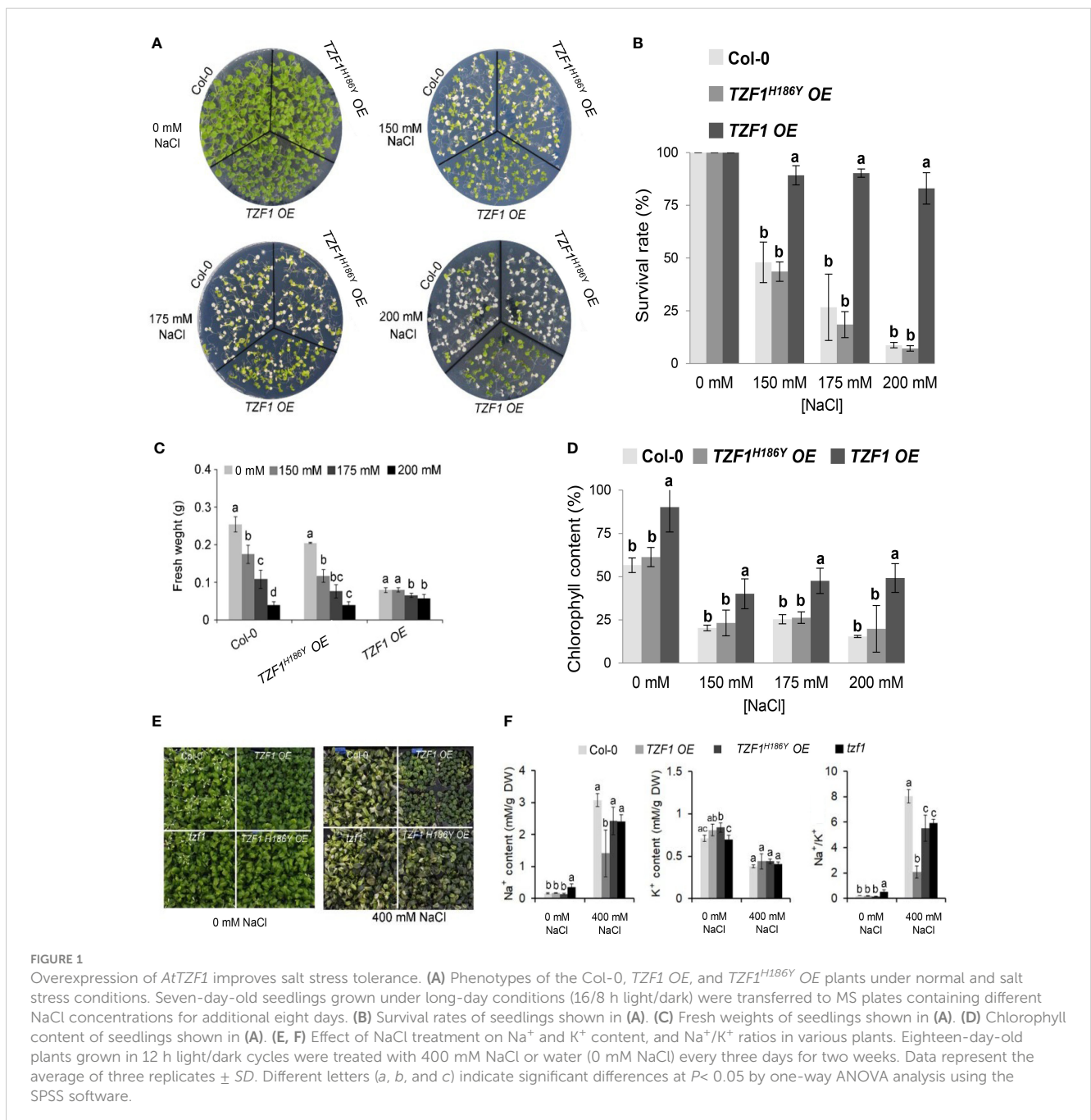### TZF1 is involved in salt stress tolerance

Previous studies have shown that *TZF1* transcription was up-regulated by high salt and that *TZF1* overexpression plants enhanced salt stress tolerance by regulating cellular ion balance and limiting oxidative and osmotic stress (Han et al., 2014). To further investigate the underlying mechanism of TZF1 in enhancing plant salt stress tolerance and determine whether the RNA-binding ability of TZF1 is required for enhancing salt stress tolerance, *Arabidopsis* plants overexpressing wild-type TZF1 (*TZF1 OE; CaMV35S:TZF1-GFP*) (Lin et al., 2011) and TZF1 mutant containing a histidine to tyrosine substitution in its second zinc finger motif (*TZF1^{H186Y} OE; CaMV35S:TZF1^{H186Y}-GFP*) (Li et al., 2019) were employed in this study. The *TZF1^{H186Y} OE* mutant allele was obtained from a genetic screen of ethyl methanesulfonate (EMS)-mutagenized *TZF1 OE* homozygous population and was isolated as a *TZF1 OE* intragenic mutant of the transgene *CaMV35S:TZF1-GFP*. Notably, *TZF1 OE* plants exhibit dwarf and late flowering while *TZF1^{H186Y} OE* plants are morphologically similar to wild-type (Col-0) plants with normal flowering time. The reversion of the overexpression phenotypes is likely due to loss-of-function of the mutated transgene *CaMV35S: TZF1^{H186Y}-GFP*, as evidenced by a previous study (Li et al., 2019).

Wild-type, *TZF1 OE*, *TZF1^{H186Y} OE*, and *tzf1* T-DNA knockout seedlings were transferred to MS medium with or without NaCl or sorbitol treatment. Under salt stress (200 mM NaCl), the survival rate, fresh weight, and chlorophyll content of the wild-type, *tzf1*, and *TZF1^{H186Y} OE* seedlings were significantly reduced, and most

seedling leaves showed bleached phenotypes. In contrast, the survival rate and chlorophyll content of *TZF1 OE* were significantly higher than those of the other plants (Figures 1A-D; Supplementary Figure 1). No significant differences in the leaf bleach phenotypes were observed among plants treated with 300 mM or 400 mM sorbitol (Supplementary Figure 2), indicating that TZF1 is more likely to be involved specifically in salt stress response but not general osmotic stress response. To further confirm that *TZF1^{H186Y} OE* conferred a revertant phenotype of *TZF1 OE*, we recapitulated the mutagenesis event by overexpressing *TZF1^{H186Y}* directly in the wild-type background under the control of the *CaMV 35S* promoter. Upon treatment with 200 mM NaCl, *TZF1^{H186Y} OE*

*L8* seedlings exhibited a high mortality rate (Supplementary Figure 3) as was found in the original EMS allele of *TZF1^{H186Y} OE*.

Under salt stress, plants utilize specific mechanisms to modulate $Na^+/K^+$ homeostasis. Thus, a low cytosolic $Na^+/K^+$ ratio is a key indication of salt stress tolerance (Zhao et al., 2021). $Na^+$ and $K^+$ concentrations and the $Na^+/K^+$ ratio were measured in leaves of *Arabidopsis* plants subjected to 400 mM NaCl in soil for 14 days. Under such treatment, growth of the wild-type, *tzf1*, and *TZF1^{H186Y} OE* plants was inhibited, while *TZF1 OE* had fewer withered yellow leaves compared to the other plants (Figure 1E). Moreover, *TZF1 OE* plants showed a reduced accumulation of $Na^+$ ions and exhibited a lower intracellular $Na^+/K^+$ ratio during salt stress



**FIGURE 1**
Overexpression of *AtTZF1* improves salt stress tolerance. **(A)** Phenotypes of the Col-0, *TZF1 OE*, and *TZF1^{H186Y} OE* plants under normal and salt stress conditions. Seven-day-old seedlings grown under long-day conditions (16/8 h light/dark) were transferred to MS plates containing different NaCl concentrations for additional eight days. **(B)** Survival rates of seedlings shown in **(A)**. **(C)** Fresh weights of seedlings shown in **(A)**. **(D)** Chlorophyll content of seedlings shown in **(A)**. **(E, F)** Effect of NaCl treatment on $Na^+$ and $K^+$ content, and $Na^+/K^+$ ratios in various plants. Eighteen-day-old plants grown in 12 h light/dark cycles were treated with 400 mM NaCl or water (0 mM NaCl) every three days for two weeks. Data represent the average of three replicates $\pm$ SD. Different letters (*a*, *b*, and *c*) indicate significant differences at $P < 0.05$ by one-way ANOVA analysis using the SPSS software.

compared to wild-type plants (Figure 1F). These results indicate that *TZF1* overexpression results in high salt-stress tolerance, suggesting that TZF1 functions as a positive regulator of salt-stress tolerance in *Arabidopsis*.

## *TZF1* overexpression alleviates oxidative damages caused by salt stress

The production of hydrogen peroxide ($H_2O_2$), a major reactive oxygen species (ROS) induced by salt stress, is an indicator of oxidative damage. To further assess the role of TZF1 in salt stress response, *TZF1 OE*, *TZF1$^{H186Y}$ OE*, and wild-type seedlings as well as adult plant leaves were stained with 3,3'-diaminobenzidine (DAB) to determine the $H_2O_2$ levels under normal and stress conditions. Under normal growth conditions, all plants leaves showed no differences in the degree of DAB staining. However, in the presence of 175 mM NaCl, the staining intensity of the *TZF1 OE* plants was significantly lower than that of the wild-type and

*TZF1$^{H186Y}$ OE* plants (Figure 2). These results indicate that $H_2O_2$ accumulation in the wild-type and *TZF1$^{H186Y}$ OE* plant leaves was greater than that in the *TZF1 OE* plants during salt stress and suggest that *TZF1* overexpression enhanced salt tolerance by reducing ROS accumulation.

## Salt-induces TZF1 stress granule assembly

Previous studies showed that TZF1 could colocalize with both PB and SG markers in *Arabidopsis* protoplasts. TZF1 localized to cytoplasmic foci in intact plants and these cytoplasmic granules can be induced by either wounding or MeJA treatment (Pomeranz et al., 2010). Moreover, OsTZF1 cytoplasmic foci could be induced by NaCl treatment (Jan et al., 2013). To investigate if TZF1 cytoplasmic foci could be induced by high salt as well, we examined seven-day-old seedlings of *TZF1 OE* and *TZF1$^{H186Y}$ OE* root cells with or without 200 mM NaCl treatment at 4 h and 24 h. Results showed that NaCl treatment could induce the formation of cytoplasmic foci
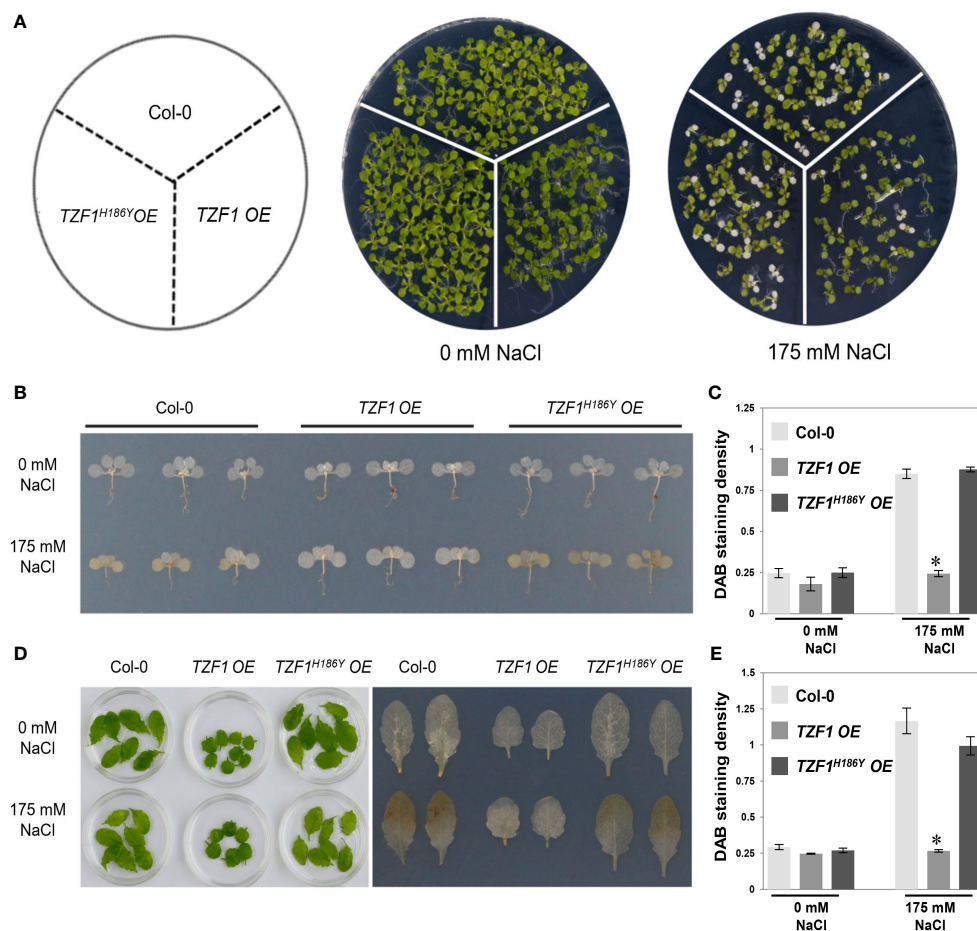


FIGURE 2
*TZF1 OE* plants accumulate less $H_2O_2$ under salt stress. **(A)** Phenotypes of the Col-0, *TZF1 OE*, and *TZF1$^{H186Y}$ OE* under normal and stress conditions. Seven-day-old seedlings grown under long-day conditions were transferred to MS plates containing 175 mM NaCl for another five days. **(B)** DAB staining to determine the levels of $H_2O_2$ accumulation in various seedlings shown in **(A)**. **(C)** Quantitative analysis of DAB staining as shown in **(B)**. **(D)** DAB staining to determine the $H_2O_2$ accumulation levels in the detached leaves of eighteen-day-old plants grown in soil under 12 h light/dark cycles treated with 175 mM NaCl or water (0 mM NaCl) for additional three days. **(E)** Quantitative analysis of DAB staining as shown in **(D)**. Data represent the average of three replicates ± SD. Asterisk indicates a significant difference (*, $P < 0.05$ by Student's *t* test).

in both *TZF1 OE* and *TZF1^{H186Y} OE* plants (Figure 3). Although there was a significant induction in number, but the size of the cytoplasmic foci were similar (Supplementary Figure 4). Interestingly, salt-induced TZF1-GFP foci appeared to be more abundant at 24 h in *TZF1^{H186Y} OE* plants than *TZF1 OE* plants, suggesting that TZF1^{H186Y}-GFP protein might be more stable, albeit non-functional, in salt stress tolerance. As the green auto-fluorescence from the cytoplasm of the light-grown seedlings interfered with the observation of GFP foci, etiolated seedlings were further examined. Again, the results confirmed that TZF1-GFP foci were salt-inducible. Consistently, both diffuse GFP and cytoplasmic granule signals were stronger in *TZF1^{H186Y} OE* plants

than that in *TZF1 OE* plants before and after NaCl treatment (Supplementary Figure 5).

Although OsTZF1 cytoplasmic foci were induced by salt stress, the identities of the foci were unknown (Jan et al., 2013). We have shown previously that TZF1 could completely co-localize with both PB (DCP2) and SG (PABP8) markers (Pomeranz et al., 2010). It was therefore confusing whether TZF proteins are components of PBs, SGs, or both. Subsequently, it was found that although plant DCP2 is a major component of mRNA decapping complex, it was not a PB-specific marker (Motomura et al., 2014), raising the possibility that TZF1 might be mainly localized in SGs and could be recruited or exchanged to PBs in response to specific cues. To test this
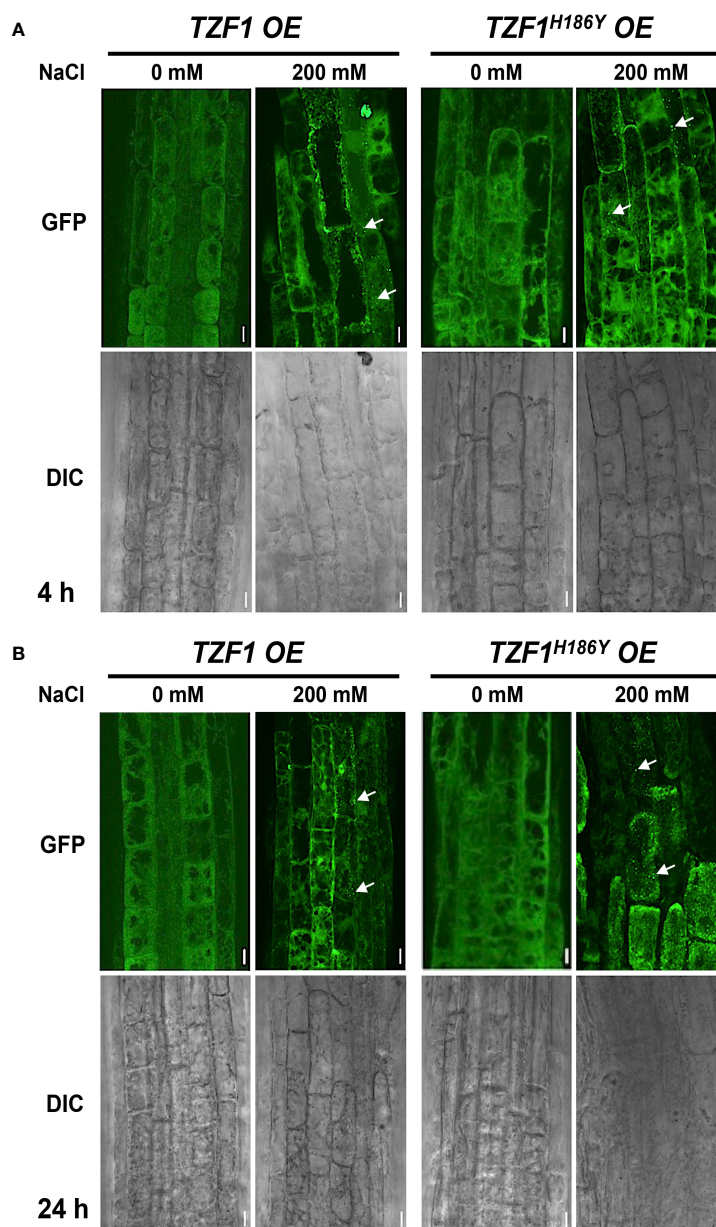


FIGURE 3
TZF1 cytoplasmic foci induced by salt stress. (A, B) Confocal microscopy of root cells of seven-day-old *TZF1 OE* and *TZF1^{H186Y} OE* seedlings treated with 200 mM NaCl for 4 h (A) and 24 h (B), respectively. GFP signals were generated by the expression of *CaMV35S:TZF1-GFP* and *CaMV35S: TZF1^{H186Y}-GFP* fusion genes. Typical TZF1 cytoplasmic foci are indicated by arrows. Salt-induced cytoplasmic foci appeared to be more abundant in *TZF1^{H186Y} OE* plants, particularly after 24 h treatment. Scale bars = 10 μm. Shown are representative results from one of the three biological replicates.

hypothesis, TZF1 sub-cellular localization was re-examined using a set of different markers in *Arabidopsis* protoplast transient expression analyses (Sheen, 2001). Results showed that TZF1 did not, or only very partially, co-localize with authentic PB markers DCP1 and DCP5, respectively, but completely co-localize with SG markers G3BP and UBP1b (Sorenson and Bailey-Serres, 2014; Jang et al., 2020; Solis-Miranda et al., 2023). Importantly, both TZF1-GFP and TZF1$^{H186Y}$-GFP were completely co-localized with SG marker UBP1b (Figure 4A). To determine if the difference in protein abundance in intact plants was specific to fusion proteins with GFP tag, *TZF1-mCherry* and *TZF1$^{H186Y}$-mCherry* were independently expressed in *Arabidopsis* protoplasts. Results showed that the signal of TZF1$^{H186Y}$-mCherry was still much stronger than TZF1-mCherry (Figure 4B).

To further determine if the salt induction of TZF1 SG assembly was a result of change in protein abundance, immunoblot analysis using eleven-day-old seedlings was conducted. Results showed that the protein level of either TZF1-GFP or TZF1$^{H186Y}$-GFP was unaffected by salt treatment and remained nearly the same (Figure 5A). Therefore, salt-induced TZF1 SG assembly is likely mediated by unknown post-translational regulatory mechanisms. Noticeably, TZF1$^{H186Y}$-GFP accumulated at a higher level than TZF1-GFP before and after salt treatment (Figure 5B). To determine protein stability, time-course analysis using seven-day-old seedlings treated with protein synthesis inhibitor cycloheximide (CHX), proteosome inhibitor MG115/132, and a combination of CHX and MG115/132 was conducted. Results showed that TZF1 protein was extremely unstable—it almost completely disappeared after seedlings were treated with CHX for just 1 h. In contrast, TZF1 accumulation was enhanced by MG115/132. Additionally, TZF1 protein even at 1 h, had already been degraded nearly 50%, suggesting that the slow action of MG132/115 treatment could not prevent the fast turnover of TZF1. This fate of TZF1 was evidenced by the combined CHX and MG115/132 treatment in which TZF1 had
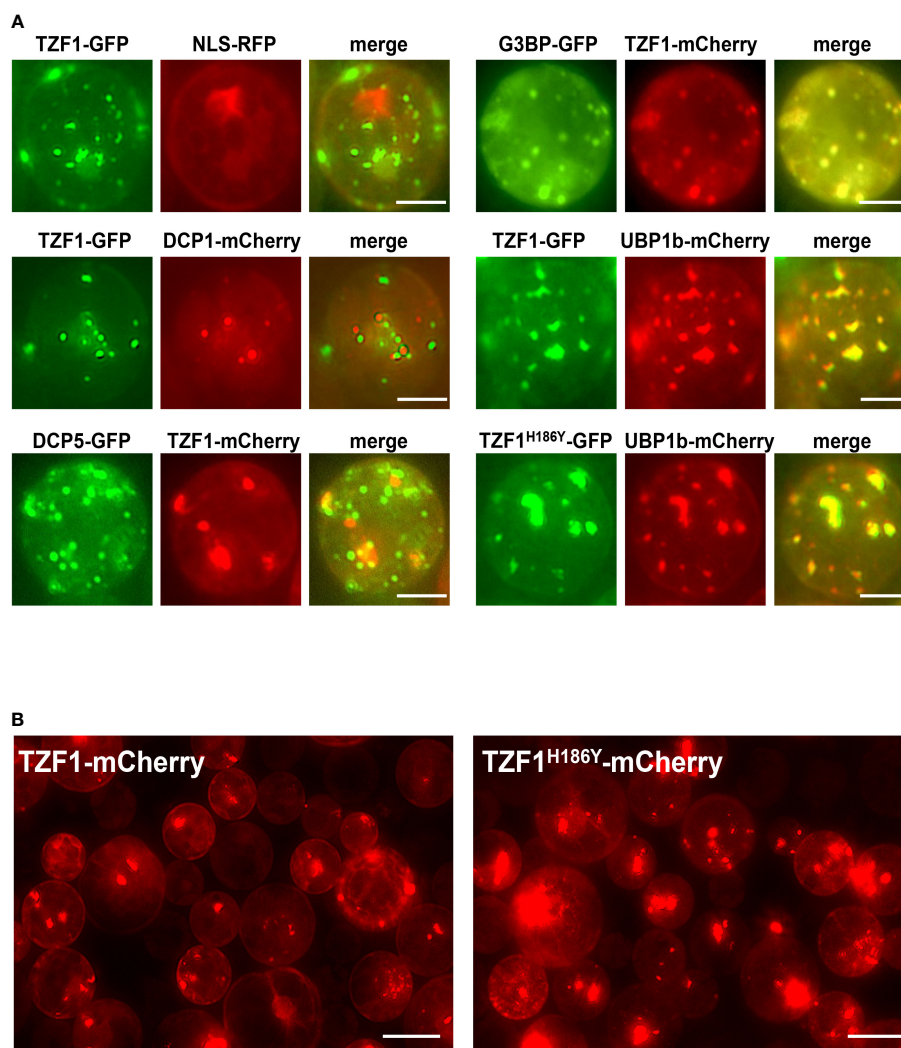


FIGURE 4
TZF1 is localized in SGs and PBs. **(A)** Individual pair of reporter constructs were co-expressed in *Arabidopsis* protoplasts. TZF1 was not colocalized with P-body marker DCP1, partially co-localized with DCP5, and completely co-localized with SG markers G3BP or UBP1b. Scale bars = 10 μm. **(B)** Cytoplasmic granules were more abundant in cells expressing TZF1$^{H186Y}$-mCherry than TZF1-mCherry. Scale bars = 20 μm. Shown are representative results from one of the three biological replicates.
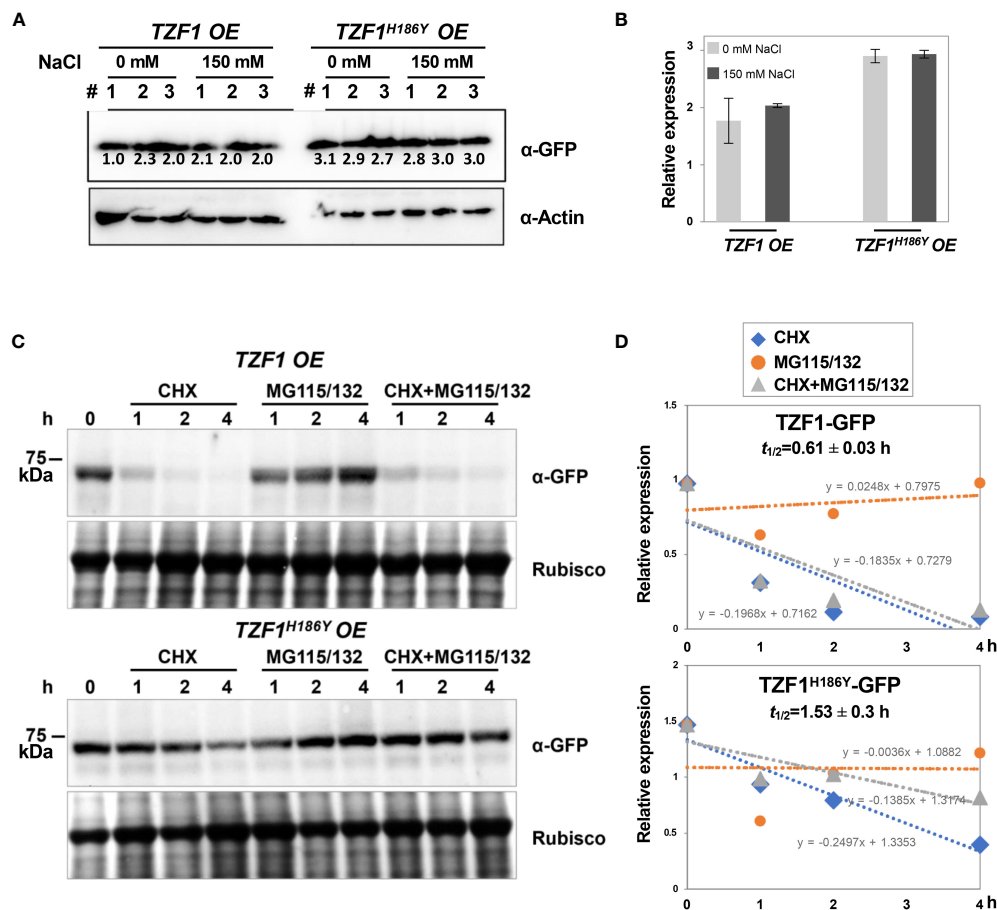
**FIGURE 5**

TZF1-GFP is less stable than TZF1[H186Y]-GFP. **(A)** Immunoblot analysis of TZF1-GFP (from *TZF1 OE* plants) and TZF1[H186Y]-GFP (from *TZF1[H186Y] OE* plants) under salt treatment. Eleven-day-old *TZF1 OE* and *TZF1[H186Y] OE* seedlings were treated with 0 mM and 150 mM NaCl for 4 h. The numbers indicate three independent samples for each treatment. The expression of ACTIN protein was used as a loading control. The number below each protein band is normalized value of GFP vs ACTIN signal. Note that the low value of the first sample is due to the smear of the ACTIN band. **(B)** Quantitative analysis of average protein bands as shown in **(A)**. Columns represent means ± SD. No statistical differences were found between 0 mM and 150 mM NaCl treatments in either *TZF1 OE* or *TZF1[H186Y] OE* plants by Student's t test ($P < 0.05$). **(C)** Half-life analysis to determine protein stability. Seven-day-old seedlings were treated with 30 µM CHX, 50 µM MG115/132, or both CHX and MG115/132. Seedlings were collected at different time points, and then total proteins were extracted for immunoblot analysis. Rubisco was used as a loading control. Shown are representative results from one of the three biological replicates. **(D)** Quantitative analysis of protein half-lives as shown in **(C)**. The slope (m) of each line is shown in the slope-intercept equation $Y = mX + c$. Protein half-life ($t_{1/2}$) is calculated from time course samples treated with CHX.

already been degraded at 1 h before MG115/132 could protect it from being degraded (Figures 5C, D). Compared to TZF1-GFP, TZF1[H186Y]-GFP was remarkably stable (Figure 5D), confirming that the higher steady-state accumulation of TZF1[H186Y]-GFP and TZF1[H186Y]-mCherry was due to enhanced protein stability. Together, these results suggest that although TZF1[H186Y]-GFP is more stable, accumulates at higher levels, and localizes to SGs, it is non-functional in enhancing plant salt stress tolerance compared to wild-type TZF1.

## TZF1 affects salt-induced transcriptome change

To uncover the role of TZF1 in modulating transcript levels of salt stress-related genes, we performed deep sequencing of RNA extracted from the wild-type, *TZF1 OE*, and *TZF1[H186Y] OE* plants

treated with 150 mM NaCl. In total, there were nearly 1,000 up-regulated and 1176 down-regulated differentially expressed genes (DEGs) present in the *TZF1 OE* plants (Figure 6A; Supplementary Figure 6A; Supplementary Dataset 1). Gene ontology (GO) analysis based on biological process clustering of DEGs in *TZF1 OE* plants revealed that up-regulated DEGs are over-represented by genes that are subject to ubiquitin transferase activity (Supplementary Figure 6B) while down-regulated DEGs preferentially associated with response to stress and response to stimulus (Figure 6B). Although the analysis of down-regulated DEGs in *TZF1 OE* is the focus of this report, we also highlight below the nexus between the outstanding up-regulated DEGs (Supplementary Figure 6C) and salt stress tolerance (see *Discussion*). For example, Na$^+$/H$^+$ antiporters (NHXs) (Bassil et al., 2011), CBL-interacting protein kinase 8 (CIPK8) (Yin et al., 2020), RGA-LIKE3 (RGL3) (Shi et al., 2017), SCF E3 ligase (PP2-B11) (Jia et al., 2015), annexin (AnnAt1)
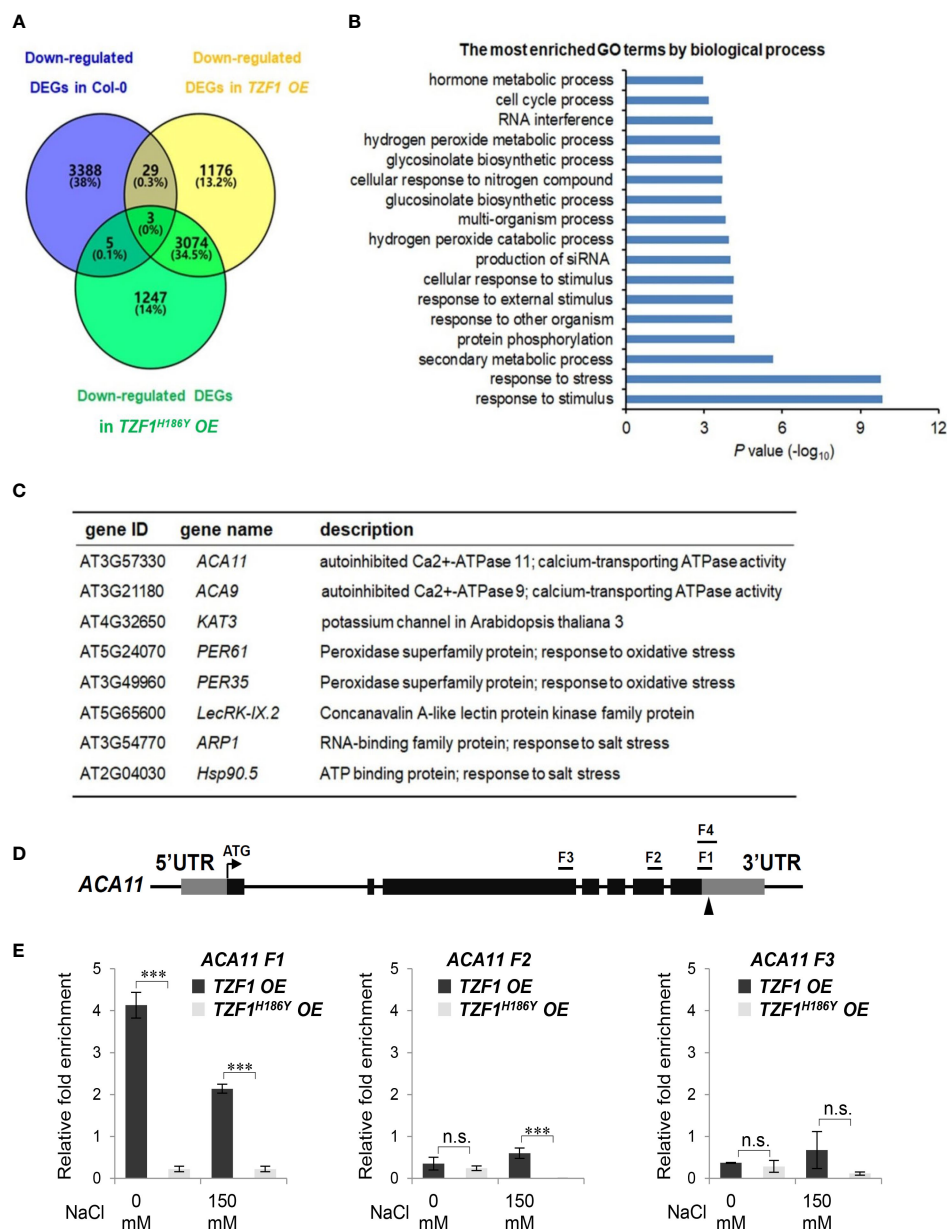
FIGURE 6

TZF1 affects salt stress responsive genes. **(A)** Venn diagram analysis of down-regulated DEGs in the Col-0, *TZF1 OE*, and *TZF1*[H186Y] *OE* plants treated with NaCl. RNA-seq analysis was conducted using eleven-day-old seedlings grown on MS plates under 12 h light/dark cycles and treated with 150 mM NaCl for 4 h. **(B)** GO analysis of down-regulated DEGs specifically found in NaCl-treated *TZF1 OE* plants. *P* values were generated by Fisher's exact test. **(C)** A set of the salt stress or oxidative stress related genes that were down-regulated in *TZF1 OE* plants and contained AU- or U-rich elements in their 3'-UTRs were selected for further analysis. **(D)** Diagram depicting the probe regions (F1 to F3) on the *ACA11* gene used for RIP-qPCR analysis. F1 and F4 fragments are mainly in the 3'-UTR region with 24 nt coding sequence upstream of the stop codon. F1 is 110 nt and F4 is an extension of F1 with 190 nt. Arrowhead indicates an ARE containing region. **(E)** RIP-qPCR results indicated a potential binding of TZF1 to the F1 region of the *ACA11* mRNA. Data represent the average of three replicates $\pm$ SD. Asterisks indicate significant differences (***, $P < 0.001$) as determined by Student's *t* test. n.s.: not significant.

(Jia et al., 2015), and vacuolar protein sorting 23A (VPS23A) (Lou et al., 2020) are all implicated as positive regulators in salt stress tolerance response.

It has been shown that the TZF motif of TZF1 is required for both RNA targeting and turnover (Qu et al., 2014). Additionally, TZF1[H186Y] could not trigger the decay of a reporter gene containing AU-rich elements (Li et al., 2019). Since the H186Y mutation is in the second zinc finger region, we tested whether the TZF region is

important for TZF1 targeting and subsequent degradation of mRNAs in response to salt stress. RNA immunoprecipitation coupled with qPCR (RIP-qPCR) was performed to determine if any of the down-regulated genes were potential direct targets of TZF1 under salt stress. Eight down-regulated DEGs in *TZF1 OE* plants were chosen from the set of salt or oxidative stress-related mRNAs containing ARE-like motifs in 3'-UTR (Figure 6C). Among these genes, the *autoinhibited Ca²⁺-ATPase* genes *ACA11* and

*ACA9* encoding calcium pumps (Li Z. et al., 2023), *KAT3* encoding a subunit of potassium channel (Sun et al., 2015), *ARP1* encoding an ABA-regulated RNA-binding protein 1 (Jung et al., 2013), and *Hsp90.5* encoding a heat shock protein (Song et al., 2009) are all implicated in negative regulation of the salt stress tolerance response. Although *ACA4* was also strongly down-regulated by salt stress in *TZF1 OE* plant in the RNA-seq analysis (Supplementary Figure 7), *ACA4* mRNA does not contain typical AREs or UREs in its 3'-UTR, and thus was not selected for further analysis. RIP-qPCR results showed that TZF1, but not the TZF$^{H186Y}$, could bind the F1 region of *ACA11* mRNA (Figures 6D, E). No significant TZF1 binding signals were detected from the rest of the seven potential target genes (Supplementary Figure 8; Supplementary Datasets 2, 3). These results indicate that *ACA11* down-regulation is a potential cause of enhanced salt stress tolerance in *TZF1 OE* plants.

## TZF1 binds *ACA11* mRNA directly

To further examine whether TZF1 binds *ACA11* mRNA directly, RNA electrophoretic mobility shift assays (EMSAs) were performed. The migration of an F4 probe, an extended derivative of the F1 region bound by TZF1 in the RIP-qPCR analysis (Figures 6D, E), was retarded by GST-TZF1 (Figure 7A). However, most of the bound complex was unable to enter the gel, so the binding affinity could not be accurately determined. Previous studies showed that both the arginine-rich (RR) and TZF domains of TZF1 were required for high-affinity ARE RNA binding (Qu et al., 2014). In addition, ARE$_{19}$ was shown to be a conserved TZF1 bound RNA motif in 3'-UTR of both plant (Qu et al., 2014) and human (Brooks and Blackshear, 2013) genes. Accordingly, recombinant MBP-TZF1 (RR-TZF) was overexpressed and purified for further EMSAs. Our results show that ARE$_{19}$ shifted readily upon incubation with increasing concentrations of MBP-RR-TZF (Supplementary Figure 9A). This clear interaction between ARE$_{19}$ and MBP-RR-TZF was leveraged in competition experiments, which were used to estimate the binding affinity of ACA11 F1, F4, and F4 deletion derivatives for TZF1. In these assays, unlabeled RNA probes were introduced as competitors to the MBP-RR-TZF–ARE$_{19}$ protein–RNA complex. The resulting gel images showed that F4 could disrupt MBP-RR-TZF binding to ARE$_{19}$ (Figure 7B). Interestingly, F4 exerted stronger competition than the F1, F4Δ84, and F4Δ134 derivatives (Figure 7C). Closer examination of the F4 nucleotide sequence revealed two U-rich segments; each of the deletion derivatives contains only one of these segments. Taken together, these results indicated that TZF1 binds *ACA11* mRNA at the 3'-UTR and that recognition of this region is dependent upon two U-rich segments in the 3'-UTR. To directly assess if TZF1$^{H186Y}$ was defective in mRNA binding, additional EMSAs were conducted. Results showed that MBP-RR-TZF$^{H186Y}$ was unable to bind the consensus ARE$_{19}$ motif (Supplementary Figure 9A) and that binding between MBP-RR-TZF$^{H186Y}$ and F4 motif was strongly impaired (Supplementary Figure 9B), suggesting that TZF1$^{H186Y}$ might be defective in mRNA binding in general.

## TZF1 enhances the degradation of *ACA11* mRNA

To investigate if reduced *ACA11* mRNA levels in *TZF1 OE* lines were due to TZF1 targeting *ACA11* mRNA for degradation, mRNA half-life analysis was conducted. An *Arabidopsis* protoplast transient expression system was used for this assay. In brief, TZF1-mCherry and TZF1$^{H186Y}$-mCherry were used as effectors and GFP-ACA11-F3 (does not bind TZF1) and GFP-ACA11-F4 (binds TZF1) were used as reporters (Figure 8A). Protoplast samples were co-transformed with a distinct effector and reporter pair and incubated for 10 h before mRNA half-life time-course experiments were conducted using actinomycin D at 0 h to block further transcription. Results showed that degradation of *GFP-ACA11-F4* mRNA was faster in the presence of TZF1 compared to TZF1$^{H186Y}$ (Figures 8B, C). In contrast, a negligible difference in *GFP-ACA11-F3* half-life was observed when it was co-expressed with either TZF1 or TZF1$^{H186Y}$, in agreement with our observation of specific binding of TZF1 to the F1/F4 region of *ACA11* in RIP-qPCR experiments (Figures 6D, E). To determine if the effectors were expressed at similar levels and the expression of the reporters correlated with corresponding mRNA half-life, we employed fluorescence microscopy. We found that the accumulation of GFP-ACA11-F4, but not GFP-ACA11-F3, was significantly reduced in the presence of TZF1 (Figure 8D), consistent with the results of mRNA half-life assays (Figures 8B, C). Immunoblot analysis further confirmed that TZF1 could specifically reduce the accumulation of GFP-ACA11-F4 protein. Note that the decay of GFP-ACA11-F4 protein was not obvious after 4 h, likely due to the accumulation and stability of the GFP protein (Figure 8E; Supplementary Figure 10). Together, these results suggest that TZF1 binds and enhances turnover of *ACA11* mRNA.

## ACA11 negatively regulates salt stress tolerance

To determine the role of ACA11 in salt stress tolerance, we compared the salt stress tolerance of wild-type and *aca11* T-DNA insertional mutant under salinity conditions. The *aca11* has the T-DNA inserted into the sixth exon of the *ACA11* (Figure 9A). RT-PCR results revealed that *ACA11* transcript was absent in homozygous *aca11* line (Figures 9B, C). In the presence of 200 mM NaCl, *aca11* seedlings showed a significantly higher survival rate than wild-type seedlings (Figures 9D, E). These results indicate that ACA11 plays a negative role in salt stress tolerance and that TZF1 targets *ACA11* mRNA for degradation to enhance salt stress tolerance.

## Discussion

Plant CCCH zinc-finger proteins play pivotal roles in abiotic stress tolerance (Han et al., 2021), but the mechanistic underpinnings are not well understood. In *Arabidopsis*, the
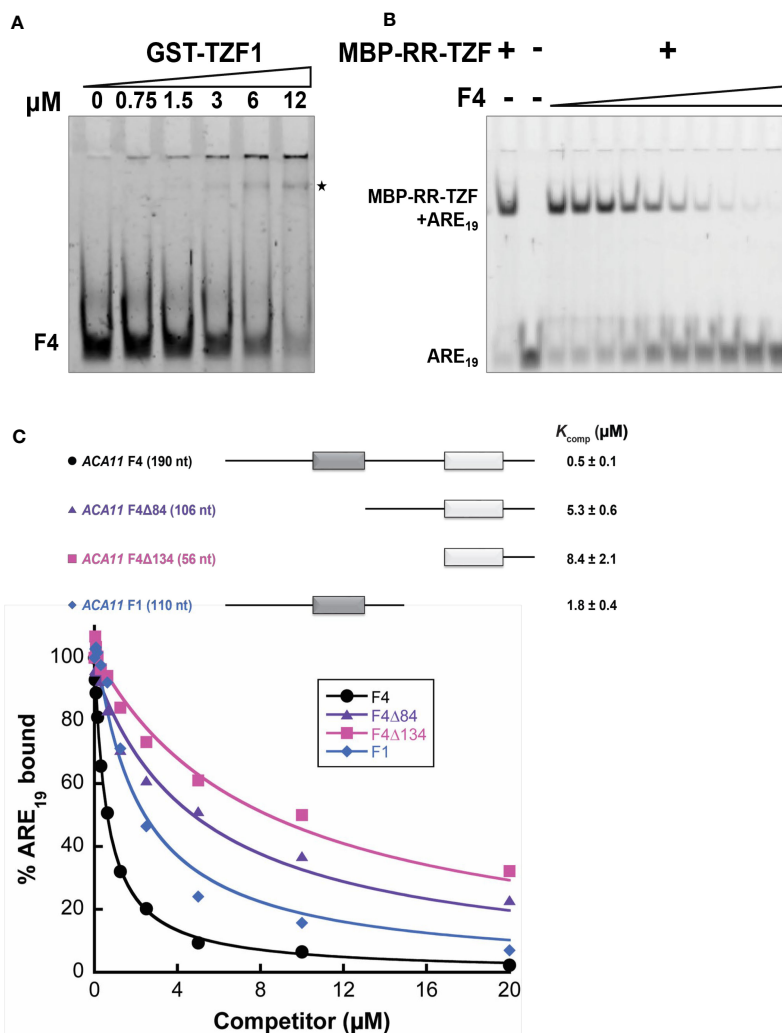
**FIGURE 7**

TZF1 binds *ACA11* mRNA. **(A)** GST-TZF1 binds the *ACA11* F4 probe region (see Figure 6D). The RNA-protein complexes are indicated by an asterisk. **(B)** Protein-RNA (MBP-RR-TZF-ARE$_{19}$) complexes are eliminated by competition with unlabeled F4 RNA probe. **(C)** Competition gel shift assays of *ACA11* F1, F4, and F4 deletion derivative RNA probes with ARE$_{19}$ RNA probe. Dark gray and light gray boxes indicate U-rich regions. A representative plot of percent ARE$_{19}$ bound versus competitor concentration is shown for each of the four RNA competitors. All reported $K_{comp}$ values and errors represent average $K_{comp}$ and standard deviation determined from three technical replicates.

expression of *TZF1/2/3/10/11* was induced by salt treatment, and overexpression of *TZF1/2/3/10/11* caused enhanced tolerance to salt stress possibly by altered expression of genes involved in biotic/abiotic stress responses (Sun et al., 2007; Lee et al., 2012; Han et al., 2014). Nevertheless, the molecular mechanisms by which TZF proteins target mRNAs to control mRNA metabolism in response to salinity stress are still unclear. In this study, knockout mutant *tzf1* showed a high salt-sensitive phenotype similar to wild-type plants, while *TZF1 OE* conferred salt stress tolerance in *Arabidopsis* seedlings (Figure 1; Supplementary Figure 1). Notably, *tzf1* plants did not show any obvious salt stress-hypersensitive phenotypes, consistent with previous reports of functional redundancy among the TZF family members (Lin et al., 2011). Our data establish unambiguously that TZF1 is a positive regulator of salt stress tolerance in *Arabidopsis*.

Our RNA-seq analysis revealed that many stress-related genes are differentially expressed between wild-type and *TZF1 OE* plants

(Figures 6A, B). A significant number of down-regulated DEGs were related to several abiotic stress-related biological processes including "response to stress" and "response to stimulus". Down-regulation of such genes is likely to engender the enhanced salt stress tolerance observed in *TZF1 OE* plants. One potential candidate is *ACA11* (Figure 6C), a tonoplast-localized Ca$^{2+}$ pump (like *ACA4*) (Li Z. et al., 2023). Salt stress is known to result in Ca$^{2+}$ accumulation in the cytoplasm where it functions as an important secondary messenger to trigger a complex signal transduction pathway to enhance salt stress tolerance (Zhao et al., 2021). Countering this flux, ACA11 and ACA4 expel Ca$^{2+}$ from the cytoplasm to vacuoles, thereby acting as negative regulators for Ca$^{2+}$ accumulation and dampening the salt-stress protective response. Consistent with this function, the double-knockout *aca4/aca11* leaves exhibit elevated baseline cytoplasmic Ca$^{2+}$ levels (Hilleary et al., 2020). The transcript level of *ACA11* was reduced in *TZF1 OE* (Figure 6), and both *TZF1 OE* plants and *aca11*
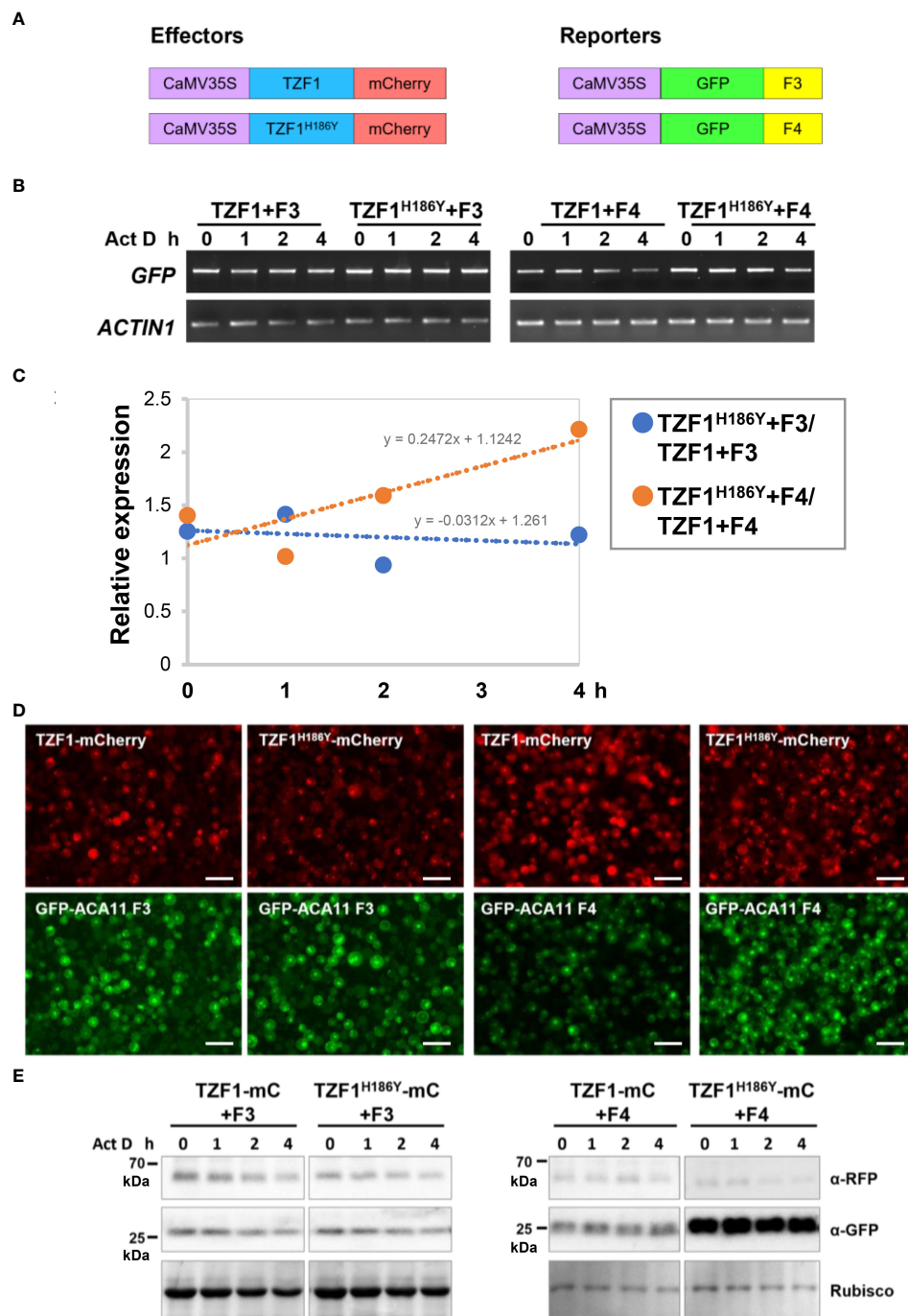
FIGURE 8
TZF1 triggers turnover of *ACA11-F4* mRNA. **(A)** Constructs used for mRNA half-life analysis. **(B)** Results of RT-PCR analysis indicate that TZF1 can enhance the degradation of *ACA11-F4*. Act D: Actinomycin D. **(C)** Quantitative analysis of mRNA half-lives with decay rates of TZF1$^{H186Y}$+Fn/TZF1+Fn as shown in **(B)**. The slope (m) of each line is shown in the slope-intercept equation Y = mX + c. **(D)** Arabidopsis protoplasts were co-expressed with a distinct pair of effector (TZF1-mCherry or TZF1$^{H186Y}$-mCherry) and reporter (GFP-ACA11 F3 or GFP-ACA11 F4). Fluorescence images were taken from each co-expressed sample using the red channel for mCherry and the green channel for GFP expression. Scale bars = 40 μm. **(E)** Results of the immunoblot analysis indicate that GFP-ACA11-F4 protein is lower when co-expressed with TZF1 than with TZF1$^{H186Y}$. Rubisco protein revealed by coomassie blue staining was used as a loading control. Shown are representative results from one of the three biological replicates.
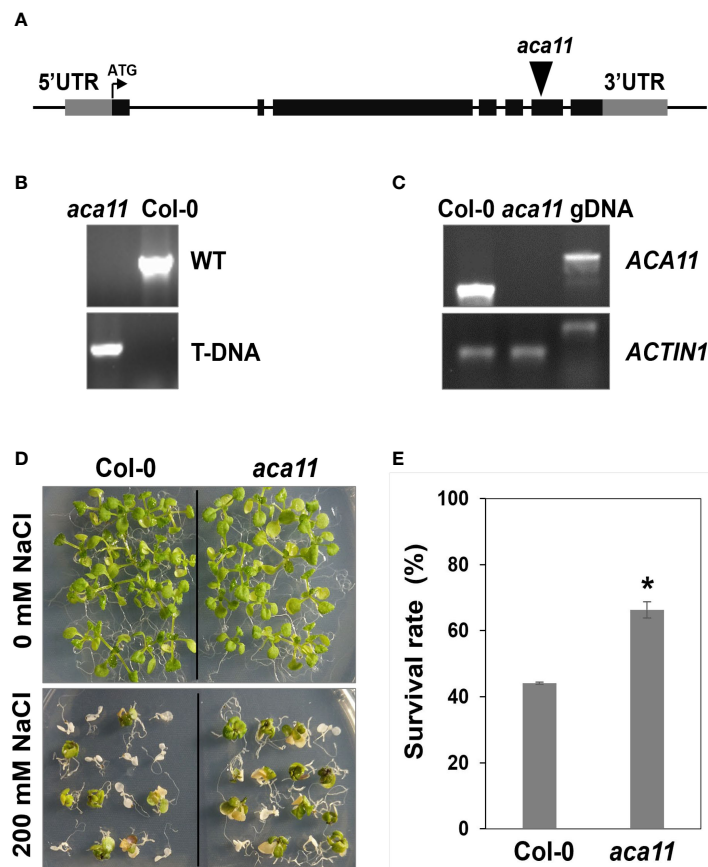
FIGURE 9

ACA11 acts as a negative regulator of salt stress tolerance. **(A)** Schematic representation of T-DNA insertion in the *ACA11* gene. **(B)** PCR genotyping analysis showing that *aca11* plant was homozygous for T-DNA insertion. Specific primers were used to detect the wild-type fragment and the T-DNA insertion, respectively, in the *ACA11* genomic locus. **(C)** Results of RT-PCR analysis indicated that *aca11* was a null mutant devoid of *ACA11* transcript. **(D)** The *aca11* seedlings showed enhanced salt stress tolerance than the wild-type plants. Plants were grown on MS plates for seven days, transferred onto MS medium supplemented with 200 mM NaCl and grown for an additional five days. **(E)** Survival rates of seedlings shown in **(D)**. Columns represent means $\pm$ SE (n > 20). Asterisk indicates a significant difference (*, $P < 0.05$) by Student's *t* test.

mutants with reduced *ACA11* expression displayed an enhanced salt stress tolerance phenotype (Figures 1 and 9). These results indicate that TZF1 positively regulates salt stress tolerance in Arabidopsis, partly by down-regulating *ACA11* through mRNA binding and degradation in *Arabidopsis*. To determine whether TZF1 is involved in mRNA turnover of target genes, we searched for ARE motifs in the down-regulated genes in *TZF1 OE* plants under salinity stress. Although we found eight genes containing typical ARE/URE motifs in their 3'-UTR (Figure 6C), we focused our attention on *ACA11*. Our results showed that TZF1 could bind *ACA11* mRNA in specific U-rich regions in its 3'-UTR both *in vivo* and *in vitro* (Figures 6E and 7). We further demonstrated that TZF1 binds both ARE and *ACA11* 3'-UTR with higher affinities than TZF1$^{H186Y}$ (Supplementary Figure 9). Using mRNA half-life analysis, we established a correlation between TZF1 binding and enhanced mRNA degradation (Figure 8). Interestingly, we found that *ACA4* was also strongly down-regulated by salt stress in *TZF1 OE* but not *TZF1$^{H186Y}$ OE* plants in the RNA-seq analysis (Supplementary Figure 7). Although *ACA4* does not contain typical AREs or UREs at 3'-UTR, we cannot rule out the possibility that TZF1 could also bind *ACA4* and trigger mRNA degradation.

Our results also inspire many future investigation avenues that are likely to be profitable. *First*, like *ACAs*, *KAT3* (*AtKC1*), a potassium channel protein, was also down-regulated in *TZF1 OE* plants (Figure 6C). As mentioned earlier, the low cytosolic Na$^+$/K$^+$ ratio is a key indication of salt stress tolerance (Zhao et al., 2021). One of the natural mechanisms of enhancing salt stress tolerance is to retain high K$^+$ levels in the cytoplasm (Sun et al., 2015). KAT3 acts as a regulatory subunit within the heterotetrameric (KAT3, KAT1, KAT2, and AKT2) potassium channel, reducing the K$^+$ conductance and negatively shifting the potassium channel activation potential (Jeanguenin et al., 2011). Therefore, down-regulation of *KAT3* in *TZF1 OE* plants could potentially activate the potassium channel and maintain high cytoplasmic K$^+$ levels to enhance salt stress tolerance. Other than *ACAs* and *KAT3*, the down-regulation of *ARP1* and *Hsp90.5* (Figure 6C) might also contribute to salt stress tolerance in *TZF1 OE* plants. Aberrant expression of *ARP1* delayed seed germination under ABA, high salt, or dehydration stress conditions (Jung et al., 2013), while

overexpression of *AtHsp90.5* reduced tolerance to both salt and drought stresses (Song et al., 2009). Additional experimentation is necessary to parse the individual contributions of these different players.

*Second*, based on the inventory of up-regulated DEGs which include several positive regulators of plant salt stress tolerance (Supplementary Figure 6C), we hypothesize that TZF1 might target the degradation of mRNAs that encode repressors of these positive regulators. For example, the *NHX* gene family contributes to $Na^+$ homeostasis in plants and plays an important role in conferring salinity tolerance (Fang et al., 2021). *NHX1* encodes a vacuolar sodium/proton antiporter involved in salt tolerance and ion homeostasis. Overexpression of *NHX1* improved salt tolerance in transgenic plants of several species (Apse et al., 1999; Zhang and Blumwald, 2001; Apse and Blumwald, 2007; Kumar et al., 2017). *NHX2* encodes a vacuolar $K^+/H^+$ exchanger essential for active $K^+$ uptake at the tonoplast. Overexpression of Jerusalem artichoke *NHX2* in rice improved salt stress tolerance (Zeng et al., 2018). *NHX6* encodes an endosomal $Na^+/H^+$ antiporter, double knockout *nhx5nhx6* showed increased sensitivity to salinity (Bassil et al., 2011). For the rest of the genes listed in (Supplementary Figure 6C), the *AtPP2-B11* plays an important role in response to salt stress by up-regulating *AnnAt1* expression, repressing ROS production, and disrupting $Na^+$ homeostasis in *Arabidopsis* (Jia et al., 2015). Under salt stress, *VPS23A* positively regulates the redistribution of SOS2 protein, also known as CIPK24, to the plasma membrane, which then activates the $Na^+/H^+$ antiporter SOS1 (known as NHX7) to exclude excess cytoplasmic $Na^+$ and confer salt stress tolerance in plants (Lou et al., 2020). Salt-induced stabilization of RGL3 by nitric oxide (NO) confers enhanced salt stress resistance (Shi et al., 2017). *CIPK8* is involved in regulating plant salt tolerance by promoting $Na^+$ export from cells (Yin et al., 2020).

*Last*, a more complete cell biological study on TZF-mRNA interaction and target mRNA metabolism is necessary. Plant TZF proteins can localize to PBs or SGs and bind specific RNA elements to trigger RNA degradation. However, very few *in vivo* mRNA binding targets have been identified to date. TZF1 was shown to localize in PBs and SGs and could trigger ARE-containing mRNA degradation *in vivo* (Pomeranz et al., 2010; Qu et al., 2014). In addition, TZF1 negatively regulates TOR signaling by binding to the 3'-UTR and promoting *TOR* mRNA degradation (Li et al., 2019). OsTZF1 and OsTZF7 can bind mRNAs of down-regulated genes containing U-rich and ARE-like motifs within their 3'-UTRs (Jan et al., 2013; Guo et al., 2022). Cotton GhTZF2 is localized to cytoplasmic granules, and transcriptome analysis showed that many differentially expressed transcripts were enriched with AREs in their 3'-UTRs, suggesting that GhTZF2 might regulate mRNA turnover of target genes (Li Y. et al., 2023). Tomato TZF protein SIC3H39 could colocalize with PB marker DCP2 and SG marker PABP8. It negatively regulates cold stress tolerance by binding to the 3'-UTR AREs and triggering degradation of the cold-responsive mRNAs (Xu et al., 2023). Despite numerous studies consistently implying that TZF proteins enhance abiotic stress response by degrading target mRNAs, the molecular details between the steps of mRNA targeting and degradation are missing. In this report, we have unequivocally determined that

TZF1 protein is mainly localized in SGs (Figure 4). Whether or not the degradation of target mRNAs takes place in SGs, PBs, or both remains an important question to address in the future. Nevertheless, we have demonstrated that both TZF1 and TZF1[H186Y] accumulate in SGs under salinity stress (Figure 3; Supplementary Figure 5), suggesting that localization of TZF1 to cytoplasmic granules might not be a sole prerequisite for its function in regulating the fates of target mRNAs. The subcellular localization and function of TZF1 in salt stress tolerance might be regulated through different mechanisms. Through deletion and site-directed mutagenesis analyses, we found that TZF1 localization to SGs is controlled by multiple domains and numerous post-translational modification mechanisms (data not shown). For example, TZF1 protein without the TZF domain could still be localized to SGs, suggesting that the mechanisms governing subcellular localization and RNA binding and/or decay could be uncoupled. Consistently, findings from both this and previous reports (Qu et al., 2014) indicate that the RR-TZF motif is responsible for RNA binding activity. By contrast, deletion of IDRs from TZF1 significantly reduced its assembly into SGs. Whether or not these IDR deletion TZF1 mutants could still confer salt stress tolerance remains an outstanding future task.

In retrospect, the higher abundance of cytoplasmic granules observed in *TZF1[H186Y]* OE plants could be due to the following possibilities: *1*) TZF1[H186Y]-GFP protein is more stable than TZF1-GFP protein (Figures 3, 5; Supplementary Figure 5). It is remarkable that a single amino acid change could change TZF1 from being extremely labile to relatively stable (Figures 5C, D). *2*) TZF1[H186Y] does not bind *ACA11* but it might be capable of binding other mRNAs and be sequestered into cytoplasmic granules. *3*) TZF1[H186Y] could interact with additional mRNA binding proteins and hence be sequestered into cytoplasmic granules. Conversely, TZF1 cytoplasmic granule localization may be coupled with its function in target mRNA degradation. An alternative hypothesis for this possibility is that *ACA11* mRNA degradation by TZF1 might mainly occur in the cytoplasm, and stronger sequestration of TZF1[H186Y] to cytoplasmic granules might prevent its accessibility to the *ACA11* mRNA in the cytoplasm. Overall, the decreased ability of TZF1[H186Y] to bind to *ACA11* mRNA and promote its degradation results in higher accumulation of *ACA11* mRNA in *TZF1[H186Y]* OE plants. Details of the interplay between subcellular localization and mRNA turnover remain to be elucidated in future studies.

In conclusion, we propose that TZF1 exerts a surprisingly effective, two-pronged post-transcriptional regulatory control on the expression of a specific set of genes involved in salt stress tolerance. By downregulating the expression of vacuolar $Ca^{2+}$ pumps (*ACA11* and *ACA4*), the likelihood of salt stress alleviation and a cellular homeostasis reset is enhanced (Supplementary Figure 11). Although we lack the identity of the repressors targeted by TZF1, a second front to offset the sodium assault is its indirect contribution to increased expression of $Na^+/H^+$ exchangers which provides an off-ramp to dampen rising cytosolic $Na^+$ levels. Moving forward, this regulatory axis of TZF1-$Ca^{2+}$-salt stress response could be leveraged to improve crop salt stress tolerance. For example, plants expressing a salt-

inducible promoter fused with *TZF1* gene could enhance salt stress tolerance but bypass the developmental abnormalities caused by the constitutive expression of *TZF1* driven by a ubiquitous promoter such as *CaMV35S* (Lin et al., 2011).

# Materials and methods

## Plant materials and growth conditions

Wild-type *Arabidopsis thaliana* Columbia-0 (Col-0), *TZF1 OE*, *TZF1^{H186Y}OE*, *tzf1* (SALK_143721), and *aca11* (SALK_060930) plants were used in this study. The plant seeds were sterilized and plated on Murashige and Skoog (MS) medium (Phytotech) for 2 days at 4°C, and then transferred to a growth chamber with 16/8 h light/dark cycles at 22°C. The light intensity was 50 $\mu$mol m$^{-1}$ s$^{-1}$.

## Seedling survival assay

Seven-day-old seedlings grown on MS plates were transferred to new MS plates containing different concentrations of NaCl for another eight days under 16/8 h light/dark cycles. The seedlings with completely bleached cotyledons were counted as dead plants; all others were counted as viable plants. At least 35 seedlings were used for each treatment.

## Chlorophyll content measurement

Sixteen seedlings were placed in a 2-ml centrifuge tube and the plant fresh weight was recorded as W. To each tube, 1 ml aliquots of 80% (v/v) acetone were added to immerse the plants. The samples were then placed in the dark for 48 h at 22°C. The acetone extract was isolated and its volume was recorded as V. For each extract, absorbance at 645 nm and 663 nm was measured using a spectrophotometer (TECAN Infinite M200 Pro) and chlorophyll content was calculated using the formula $[(8.02 \times Abs_{663}) + (20.21 \times Abs_{645})] \times V/W$ as previously described (Li et al., 2021).

## Na$^+$ and K$^+$ Content Measurement

Accumulation of Na$^+$ and K$^+$ ions was measured according to a previously described (Jiang et al., 2019). Plants grown in the presence or absence of NaCl treatment were separately harvested and dried for 48 h at 65°C before their weight was measured. All samples were then digested with 75% (v/v) nitric acid and 25% (v/v) hydrogen peroxide at 180°C for 3 h. The samples were then diluted to 30 ml with ddH$_2$O and filtered. The Na$^+$ and K$^+$ contents in each solution were measured using an inductively coupled plasma optical emission spectrometer (ICAP6300).

## DAB staining

Seedlings and leaves were incubated in DAB staining solution (1 mg/ml DAB dissolved in ddH$_2$O, pH 3.8) in the dark at 22°C for 8 h. The samples were then destained with acetic acid:glycerin:ethanol

(1:1:4 by volume) at 80°C for 25 min before imaging. Images of DAB staining results were quantified by using Image J (NIH).

## RNA-seq sample preparation and sequencing

Eleven-day-old seedlings grown on MS plates under 12/12 h light/dark cycles were treated with 150 mM NaCl at Zeitgeber time (ZT)2 for 4 h before sample collection and total RNA extraction. Three biological replicates were prepared for each sample. Total RNA was extracted using Trizol reagent (Invitrogen). The RNA was then treated with DNase I (DNA-*free*$^{TM}$ DNA Removal Kit, Invitrogen) to remove genomic DNA. RNA quality was evaluated on a Bioanalyzer 2100 instrument (Agilent). Sequencing libraries were prepared using the Directional RNA Library Prep Kit (E7760S, New England Biolabs) according to manufacturer's instructions. The 150-nucleotide (nt) paired-end high-throughput sequencing was performed using an Illumina Hiseq X TEN platform. After removing the low-quality sequencing reads, the remaining clean reads were mapped to the *Arabidopsis* reference genome (TAIR10) using Tophat2 software. DEGs were analyzed using edgeR software. Genes with $q < 0.05$ and $|\log 2 \_ratio| \geq 1.5$ were identified as DEGs. The enrichment of DEGs in different functional categories was performed by using agriGO (GeneOntology) V2.0. Venn diagram analysis was conducted using VENNY 2.1. Three biological replicates were prepared for each sample. To select candidate DEGs for further analysis, there were 339 genes in the GO "response to stimulus" and 210 genes in the GO "response to stress" category. Salt stress is commonly caused by high concentrations of Na$^+$. The salt stress induced not only ionic stress but also other secondary stresses, which include the accumulation of toxic compounds such as ROS. The plant cell minimizes cellular damage by reducing cytoplasmic Na$^+$ and limiting the ROS concentration in the cell (Yang and Guo, 2018). Therefore, the genes in the GOs "response to stimulus" and "response to stress" were used for BLAST search and yielded 31 genes responding to salt stress, 12 genes involved in hydrogen peroxide catabolic process and ROS metabolic process, and 10 genes involved in inorganic cation transmembrane transport. Among these 53 genes, 8 genes containing ARE-like motifs in 3'-UTR of the mRNA were selected for the subsequent RIP-seq analysis.

## RNA immunoprecipitation (RIP) and RT-qPCR analysis

Eleven-day-old seedlings grown on MS plates under 12/12-h light/dark cycles were treated with 150 mM NaCl at ZT2 for 4 h before samples were collected for crosslinking. RIP was performed as previously described (Koster et al., 2014). Briefly, the cross-linked tissues (1.5 g) were ground with liquid nitrogen and resuspended in 750 $\mu$l prewarmed (60°C) RIP lysis buffer to make viscous homogenates. After centrifugation, the cell extract supernatant was filtered through a 0.45 $\mu$m filter. The extract was then pre-cleared twice with 50 $\mu$l Sepharose beads before mixing with 15 $\mu$l washed Sepharose beads coated with GFP antibody (Invitrogen).

The beads were incubated with extract for 2 h at 4°C and then washed three times with RIP washing buffer for 10 min at 4°C. The beads were then washed with RIP lysis buffer for 5 min at 4°C. The RNA was purified from the immunoprecipitated RNPs and 100 μl input, respectively, using the Trizol reagent (Invitrogen). For quantitative analysis of TZF1 binding to RNA, reverse transcription was performed using SuperScript$^{TM}$ IV First Strand Synthesis System. After DNase treatment, RNA samples were reverse transcribed with random hexamer primers. Quantitative PCR was performed to determine the level of TZF1-bound RNA, and the $2^{-\Delta CT}$ method was used to calculate the ratio of RIP to the input.

## TZF1 protein half-life analysis

Seven-day-old *TZF1 OE* and *TZF1$^{H186Y}$ OE* seedlings were incubated with 30 μM cycloheximide (CHX), 50 μM MG115/132, or both CHX and MG115/132. Seedlings were collected at different time points, and then total proteins were extracted and protein levels were determined by immunoblot analysis with anti-GFP antibody (Roche).

## Recombinant protein production

Recombinant GST-TZF1 and MBP-TZF1 (RR-TZF) proteins were overexpressed in *Escherichia coli* BL21 (DE3) cells. Bacterial cultures were grown to $Abs_{600}$ = 0.6, at which point 0.1 mM isopropyl β-D-1-thiogalactopyranoside (IPTG) was added for induction of protein production. ZnCl$_2$ (0.1 mM) and glucose [0.2% (w/v); MBP-RR-TZF only] were also added at the time of addition induction. Cultures were then grown for an additional 12-16 h at 18°C before harvesting. GST-TZF1 was purified using glutathione-Sepharose 4B resin (GE Healthcare Bio Sciences) as previously described (Qu et al., 2014). For purification of MBP-RR-TZF, cell pellets from a 1 L overexpression culture were resuspended in 20 ml extraction buffer [50 mM Tris-HCl, pH 8.5; 100 mM NaCl; 1 mM EDTA, 1 mM DTT, 1 mM PMSF, 0.5X EDTA-free protease inhibitor cocktail (APExBIO)]. The resuspended cells were lysed at 15,000 psi using a French pressure cell press, and the resulting whole-cell lysate was supplemented with 0.2% (v/v) Triton X-100 and incubated at 4°C for 10 min with gentle nutation. The lysate was then supplemented with 10 mM MgCl$_2$ and 10 mM CaCl$_2$ and 5 μg DNase I (Sigma-Aldrich) and incubated at 20°C for an additional 10 min. After incubation, the lysate was clarified by centrifugation at 12,000 x *g* and 4°C for 15 min and then filtered using a 0.45-μm syringe filter (Roche). The filtered lysate was passed over a gravity-flow column packed with 0.5 ml amylose resin (New England Biolabs) that had been pre-equilibrated with extraction buffer. After collecting the flowthrough, the amylose resin was washed with 20 ml extraction buffer to remove weakly bound proteins. Bound MBP-RR-TZF was eluted with 0.5 ml additions of elution buffer (50 mM Tris-HCl, pH 8.5, 10 mM amylose, 1 mM DTT) and individual elution fractions were collected and assessed by SDS-PAGE. The fractions containing

near-homogeneous MBP-RR-TZF were pooled and dialyzed twice against 500 ml storage buffer (20 mM Tris-HCl, pH 8.0; 50 mM NaCl; 1 mM DTT) at 4°C. The final protein concentration was determined by measuring $Abs_{280}$ (ε = 81,820 M$^{-1}$ cm$^{-1}$). Prior to use in competition assays, aliquots of MBP-RR-TZF were concentrated to ~80 μM using a Vivapsin 500 10,000 MWCO centrifugal concentrator (Sartorius). All protein aliquots were stored at -80°C.

## Preparation of RNAs

The F4, F4Δ84, F4Δ134, and F1 RNAs were generated by run-off *in vitro* transcription (IVT) using T7 RNA polymerase. The DNA templates for IVT were prepared by PCR using cDNA as the template. The F4, F4Δ84, and F4Δ134 IVT templates were amplified using F4-F, F4Δ84-F, and F4Δ134-F forward primers, respectively, and F4-R as the common reverse primer. Due to poor amplification of the F4Δ134 template after the first PCR, the amplicon from the first round was used as the template in a second PCR that used the same set of primers as in the first round. IVT reactions contained 1x IVT buffer [40 mM Tris-HCl, pH 7.6; 24 mM MgCl$_2$; 2 mM spermidine; 0.01% (v/v) Triton X-100]; 10 mM DTT; 5 mM each of ATP, CTP, GTP, and UTP; 0.002 U thermostable inorganic pyrophosphatase (NEB); 0.15-0.3 μg template, and T7 RNA polymerase (purified in-house)]. After 4 h at 37°C, the reactions were treated with DNase I (Roche), extracted with phenol-chloroform, and dialyzed using 3,500-MWCO tubing (BioDesign Inc. New York) against 3.5 L ddH$_2$O three times over 20 h at 4°C and once over 1.5 h at 20°C. Following dialysis, the RNAs were precipitated with 0.3 M sodium acetate and 2.5 volumes of ethanol, resuspended in autoclaved ddH$_2$O, and quantitated by measuring the absorbance at $Abs_{260}$ and using their respective extinction coefficients (OligoAnalyzer, IDT).

To prepare 5′-[$^{32}$P]-labeled F4 (5′-[$^{32}$P]-F4), F4 was first dephosphorylated by incubating with calf intestinal phosphatase (NEB) for 2 h at 37°C. Dephosphorylated F4 was then extracted with phenol-chloroform, precipitated with sodium acetate and ethanol, and resuspended in ddH$_2$O as described above. Following clean-up, dephosphorylated F4 (5 μM) was incubated with γ-[$^{32}$P]-ATP and T4 polynucleotide kinase (NEB) for 45 min at 37°C. The labeling reaction was quenched with the addition of urea dye [7 M urea, 1 mM EDTA, 0.05% (w/v) xylene cyanol, 0.05% (w/v) bromophenol blue, 10% (v/v) phenol], loaded onto a denaturing 8% (w/v) polyacrylamide/7 M urea/1X Tris-Borate-EDTA (TBE) gel, and electrophoresed in 1X TBE buffer for 75 min. Full-length 5′-[$^{32}$P]-F4 was identified in the gel by autoradiography, excised from the gel, and eluted using the crush-and-soak method. Eluted 5′-[$^{32}$P]-F4 was precipitated with sodium acetate and ethanol and resuspended to a final specific activity of 200,000 dpm/μl in ddH$_2$O.

## Gel-shift assays

For TZF binding to ARE$_{19}$, a pre-mixed solution of 100 nM 6-FAM-labeled ARE$_{19}$ (6-FAM-ARE$_{19}$, IDT) and 40 μM 20-nt decoy oligo (MilliporeSigma) in binding buffer [20 mM HEPES-KOH, pH

7.5; 50 mM NaCl; 5 μM $ZnCl_2$, 4 mM $MgCl_2$] was aliquoted into multiple tubes. Importantly, inclusion of the 20-nt decoy oligo minimized apparent nucleolytic decay of the target RNA during the binding reaction and improved the resolution of free 6-FAM-$ARE_{19}$ bands in the gel image. MBP-RR-TZF (or H186Y mutant) was serially diluted from 40 μM to 156 nM by diluting with equal volumes of storage buffer [20 mM Tris-HCl, pH 8; 50 mM NaCl; 1 mM DTT]. To initiate the binding reaction, equal volumes of MBP-RR-TZF were combined with the pre-mixed aliquots of 6-FAM-$ARE_{19}$ and decoy oligo. As a negative control, a single aliquot of 6-FAM-$ARE_{19}$ and decoy oligo was diluted with an equal volume of storage buffer. The binding reactions were incubated at 23°C for 10 min. Loading dye containing xylene cyanol, bromophenol blue, and 50% (v/v) glycerol was added to each tube, and each reaction mix was loaded onto a native 8% (w/v) polyacrylamide (29:1 acrylamide: bisacrylamide)/1X Tris-Borate (TB) gel. The gel was electrophoresed in 1X TB buffer at 100 V for 1 h at 4°C and then scanned using an Amersham Typhoon Biomolecular Imager (Cytiva) on the Cy2 setting.

For TZF binding to ACA11-F4, a pre-mixed solution of 1 nM 5′-[$^{32}$P]-F4 and 40 μM 20-nt decoy oligo in binding buffer was aliquoted into multiple tubes. MBP-RR-TZF (or H186Y mutant) was serially diluted from 40 μM to 156 nM by diluting with equal volumes of storage buffer. To initiate the binding reaction, equal volumes of MBP-RR-TZF were combined with the pre-mixed aliquots of 5′-[$^{32}$P]-F4 and decoy oligo. The binding reactions were incubated and resolved by native polyacrylamide gel electrophoresis as described for 6-FAM-$ARE_{19}$, except the binding reactions were resolved on a 6% (w/v) polyacrylamide/1X TB gel, and the gel was exposed to storage phosphor screen which was then scanned using an Amersham Typhoon Biomolecular Imager (Cytiva) on the phosphorimager setting.

## Competition gel shift assays

The binding affinity of MBP-RR-TZF for ACA11 F4 and deletion derivatives (F1, F4Δ84, F4Δ134) was measured in a gel-shift assay by monitoring dissociation of MBP-RR-TZF from 6-FAM-$ARE_{19}$, which was previously established as a minimal RNA ligand for MBP-RR-TZF (Qu et al., 2014). For all competition assays, a fixed concentration of 20 μM MBP-RR-TZF was used to ensure near-complete binding to $ARE_{19}$ in the absence of competitor RNA, and then subject to a competition with increasing concentration of either F4 or one of the F4 deletion derivatives. All reported RNA and protein concentrations reflect the final concentrations in the binding assay. A pre-mixed solution of 50 nM 6-FAM-$ARE_{19}$ and 20 μM 20-nt decoy oligo in binding buffer (20 mM HEPES-KOH, pH 7.5; 50 mM NaCl; 5 μM $ZnCl_2$, 4 mM $MgCl_2$) was aliquoted into multiple tubes and supplemented with increasing concentrations of competitor RNA. Two aliquots that were designated as positive- and negative-binding controls were supplemented with $ddH_2O$ instead of competitor RNA. To the binding reaction and positive-control tubes, 20 μM MBP-RR-TZF was added, whereas storage buffer was added to the negative control

tube. The binding reactions were incubated and resolved by native polyacrylamide gel electrophoresis as described for 6-FAM-$ARE_{19}$. Following electrophoresis, gels were scanned using an Amersham Typhoon imager (Cytiva) on the Cy2 setting, and the intensity of bands corresponding to bound and unbound 6-FAM-$ARE_{19}$ were quantified using ImageQuant software (Molecular Dynamics). The fraction of 6-FAM-$ARE_{19}$ bound at each competitor concentration was normalized using the fraction of $ARE_{19}$ bound in the positive control sample and plotted as % bound $ARE_{19}$. Data were fit to a hyperbolic binding isotherm ($[\Delta ARE_{19}$ bound]$*K_{comp}$)/ ([competitor] + $K_{comp}$) to yield the $K_{comp}$ value for binding of MBP-RR-TZF to a competitor RNA.

## Messenger RNA half-life assays

The TZF1, TZF1$^{H186Y}$, ACA11-F3, and ACA11-F4 were cloned into the pENTR$^{TM}$/D-TOPO® vectors. All constructs were subcloned into the Gateway® destination vectors with N-terminal GFP or C-terminal mCherry tag by using the LR recombination reaction. *Arabidopsis* protoplast samples were co-transformed with a distinct effector and reporter pair (TZF1+ACA11-F3, TZF1+ACA11-F4, TZF1$^{H186Y}$+ACA11-F3, TZF1$^{H186Y}$+ACA11-F4) and incubated for 10 h before mRNA half-life time-course experiments were conducted. Actinomycin D (Sigma) at 100 μg/ml was used to block the transcription at the beginning of the time-course experiments. Total RNA was extracted by using a RNeasy plant mini kit (Qiagen), then treated with TURBO DNA-*free*$^{TM}$ Kit (Ambion) to remove contaminating genomic and plasmid DNA. First-strand cDNA was synthesized by using the SuperScript III reverse transcriptase (Invitrogen) according to the supplier's instructions. *ACTIN1* was used as an internal control for RT-PCR analysis.

## Data availability statement

The original contributions presented in the study are publicly available. This data can be found here: NGDC GSA, CRA015388. https://bigd.big.ac.cn/gsa/browse/CRA015388.

## Author contributions

S-LH: Data curation, Formal analysis, Investigation, Writing – original draft, Writing – review & editing. BL: Data curation, Formal analysis, Investigation, Writing – original draft. WJZ: Data curation, Formal analysis, Investigation, Writing – review & editing. HCA: Formal analysis, Investigation, Writing – review & editing. VS: Formal analysis, Investigation, Writing – review & editing. VG: Conceptualization, Investigation, Supervision, Validation, Funding acquisition, Resources, Writing – review & editing. LW: Conceptualization, Investigation, Supervision, Validation, Funding acquisition, Resources, Writing – review & editing. J-CJ: Conceptualization, Investigation, Supervision, Validation, Funding acquisition, Resources, Writing – review & editing.

## Funding

## Acknowledgments

## Conflict of interest

The authors declare that the research was conducted in the absence of any commercial or financial relationships that could be construed as a potential conflict of interest.

The author(s) declared that they were an editorial board member of Frontiers, at the time of submission. This had no impact on the peer review process and the final decision.

## Publisher's note

## Supplementary material

The Supplementary Material for this article can be found online at: https://www.frontiersin.org/articles/10.3389/fpls.2024.1375478/full#supplementary-material

**SUPPLEMENTARY DATA SHEET 1**
Transcriptome analysis.

**SUPPLEMENTARY DATA SHEET 2**
RIP-qPCR data-1.

**SUPPLEMENTARY DATA SHEET 3**
RIP-qPCR data-2.

## References

Apse, M. P., Aharon, G. S., Snedden, W. A., and Blumwald, E. (1999). Salt tolerance conferred by overexpression of a vacuolar Na+/H+ antiport in Arabidopsis. *Science* 285, 1256–1258. doi: 10.1126/science.285.5431.1256

Apse, M. P., and Blumwald, E. (2007). Na+ transport in plants. *FEBS Lett.* 581, 2247–2254. doi: 10.1016/j.febslet.2007.04.014

Bassil, E., Ohto, M. A., Esumi, T., Tajima, H., Zhu, Z., Cagnac, O., et al. (2011). The Arabidopsis intracellular Na+/H+ antiporters NHX5 and NHX6 are endosome associated and necessary for plant growth and development. *Plant Cell* 23, 224–239. doi: 10.1105/tpc.110.079426

Blanvillain, R., Wei, S., Wei, P., Kim, J. H., and Ow, D. W. (2011). Stress tolerance to stress escape in plants: role of the OXS2 zinc-finger transcription factor family. *EMBO J.* 30, 3812–3822. doi: 10.1038/emboj.2011.270

Bogamuwa, S., and Jang, J. C. (2013). The Arabidopsis tandem CCCH zinc finger proteins AtTZF4, 5 and 6 are involved in light-, abscisic acid- and gibberellic acid-mediated regulation of seed germination. *Plant Cell Environ.* 36, 1507–1519. doi: 10.1111/pce.12084

Brooks, S. A., and Blackshear, P. J. (2013). Tristetraprolin (TTP): interactions with mRNA and proteins, and current thoughts on mechanisms of action. *Biochim. Biophys. Acta* 1829, 666–679. doi: 10.1016/j.bbagrm.2013.02.003

Carballo, E., Lai, W. S., and Blackshear, P. J. (1998). Feedback inhibition of macrophage tumor necrosis factor-alpha production by tristetraprolin. *Science* 281, 1001–1005. doi: 10.1126/science.281.5379.1001

Deinlein, U., Stephan, A. B., Horie, T., Luo, W., Xu, G., and Schroeder, J. I. (2014). Plant salt-tolerance mechanisms. *Trends Plant Sci.* 19, 371–379. doi: 10.1016/j.tplants.2014.02.001

Fang, S., Hou, X., and Liang, X. (2021). Response mechanisms of plants under saline-alkali stress. *Front. Plant Sci.* 12, 667458. doi: 10.3389/fpls.2021.667458

Guo, C., Chen, L., Cui, Y., Tang, M., Guo, Y., Yi, Y., et al. (2022). RNA binding protein OsTZF7 traffics between the nucleus and processing bodies/stress granules and positively regulates drought stress in rice. *Front. Plant Sci.* 13, 802337. doi: 10.3389/fpls.2022.802337

Han, G., Qiao, Z., Li, Y., Wang, C., and Wang, B. (2021). The roles of CCCH zinc-finger proteins in plant abiotic stress tolerance. *Int. J. Mol. Sci.* 22, 8327. doi: 10.3390/ijms22158327

Han, G., Wang, M., Yuan, F., Sui, N., Song, J., and Wang, B. (2014). The CCCH zinc finger protein gene AtZFP1 improves salt resistance in Arabidopsis thaliana. *Plant Mol. Biol.* 86, 237–253. doi: 10.1007/s11103-014-0226-5

Hilleary, R., Paez-Valencia, J., Vens, C., Toyota, M., Palmgren, M., and Gilroy, S. (2020). Tonoplast-localized Ca(2+) pumps regulate Ca(2+) signals during pattern-triggered immunity in Arabidopsis thaliana. *Proc. Natl. Acad. Sci. U.S.A.* 117, 18849–18857. doi: 10.1073/pnas.2004183117

Huang, P., Chung, M. S., Ju, H. W., Na, H. S., Lee, D. J., Cheong, H. S., et al. (2011). Physiological characterization of the Arabidopsis thaliana oxidation-related zinc finger 1, a plasma membrane protein involved in oxidative stress. *J. Plant Res.* 124, 699–705. doi: 10.1007/s10265-010-0397-3

Huang, P., Ju, H. W., Min, J. H., Zhang, X., Chung, J. S., Cheong, H. S., et al. (2012). Molecular and physiological characterization of the Arabidopsis thaliana Oxidation-related Zinc Finger 2, a plasma membrane protein involved in ABA and salt stress response through the ABI2-mediated signaling pathway. *Plant Cell Physiol.* 53, 193–203. doi: 10.1093/pcp/pcr162

Jan, A., Maruyama, K., Todaka, D., Kidokoro, S., Abo, M., Yoshimura, E., et al. (2013). OsTZF1, a CCCH-tandem zinc finger protein, confers delayed senescence and stress tolerance in rice by regulating stress-related genes. *Plant Physiol.* 161, 1202–1216. doi: 10.1104/pp.112.205385

Jang, G. J., Jang, J. C., and Wu, S. H. (2020). Dynamics and functions of stress granules and processing bodies in plants. *Plants (Basel)* 9, 1122. doi: 10.3390/plants9091122

Jang, J. C. (2016). Arginine-rich motif-tandem CCCH zinc finger proteins in plant stress responses and post-transcriptional regulation of gene expression. *Plant Sci.* 252, 118–124. doi: 10.1016/j.plantsci.2016.06.014

Jeanguenin, L., Alcon, C., Duby, G., Boeglin, M., Cherel, I., Gaillard, I., et al. (2011). AtKC1 is a general modulator of Arabidopsis inward Shaker channel activity. *Plant J.* 67, 570–582. doi: 10.1111/j.1365-313X.2011.04617.x

Jia, F., Wang, C., Huang, J., Yang, G., Wu, C., and Zheng, C. (2015). SCF E3 ligase PP2-B11 plays a positive role in response to salt stress in Arabidopsis. *J. Exp. Bot.* 66, 4683–4697. doi: 10.1093/jxb/erv245

Jiang, Z., Zhou, X., Tao, M., Yuan, F., Liu, L., Wu, F., et al. (2019). Plant cell-surface GIPC sphingolipids sense salt to trigger Ca(2+) influx. *Nature* 572, 341–346. doi: 10.1038/s41586-019-1449-z

Julkowska, M. M., and Testerink, C. (2015). Tuning plant signaling and growth to survive salt. *Trends Plant Sci.* 20, 586–594. doi: 10.1016/j.tplants.2015.06.008

Jung, H. J., Kim, M. K., and Kang, H. (2013). An ABA-regulated putative RNA-binding protein affects seed germination of Arabidopsis under ABA or abiotic stress conditions. *J. Plant Physiol.* 170, 179–184. doi: 10.1016/j.jplph.2012.09.002

Kim, D. H., Yamaguchi, S., Lim, S., Oh, E., Park, J., Hanada, A., et al. (2008). SOMNUS, a CCCH-type zinc finger protein in Arabidopsis, negatively regulates light-dependent seed germination downstream of PIL5. *Plant Cell* 20, 1260–1277. doi: 10.1105/tpc.108.058859

Kong, L., Feng, B., Yan, Y., Zhang, C., Kim, J. H., Xu, L., et al. (2021). Noncanonical mono(ADP-ribosyl)ation of zinc finger SZF proteins counteracts ubiquitination for protein homeostasis in plant immunity. *Mol. Cell* 81, 4591–4604, e4598. doi: 10.1016/j.molcel.2021.09.006

Kong, Z., Li, M., Yang, W., Xu, W., and Xue, Y. (2006). A novel nuclear-localized CCCH-type zinc finger protein, OsDOS, is involved in delaying leaf senescence in rice. *Plant Physiol.* 141, 1376–1388. doi: 10.1104/pp.106.082941

Koster, T., Haas, M., and Staiger, D. (2014). The RIPper case: identification of RNA-binding protein targets by RNA immunoprecipitation. *Methods Mol. Biol.* 1158, 107–121. doi: 10.1007/978-1-4939-0700-7_7

Kumar, S., Kalita, A., Srivastava, R., and Sahoo, L. (2017). Co-expression of Arabidopsis NHX1 and bar improves the tolerance to salinity, oxidative stress, and herbicide in transgenic mungbean. *Front. Plant Sci.* 8, 1896. doi: 10.3389/fpls.2017.01896

Lai, W. S., Carballo, E., Strum, J. R., Kennington, E. A., Phillips, R. S., and Blackshear, P. J. (1999). Evidence that tristetraprolin binds to AU-rich elements and promotes the deadenylation and destabilization of tumor necrosis factor alpha mRNA. *Mol. Cell Biol.* 19, 4311–4323. doi: 10.1128/MCB.19.6.4311

Lee, S. J., Jung, H. J., Kang, H., and Kim, S. Y. (2012). Arabidopsis zinc finger proteins AtC3H49/AtTZF3 and AtC3H20/AtTZF2 are involved in ABA and JA responses. *Plant Cell Physiol.* 53, 673–686. doi: 10.1093/pcp/pcs023

Li, B., Wang, Y., Zhang, J., Tian, W., Chong, K., Jang, J. C., et al. (2019). PRR5, 7 and 9 positively modulate TOR signaling-mediated root cell proliferation by repressing TANDEM ZINC FINGER 1 in Arabidopsis. *Nucleic Acids Res.* 47, 5001–5015. doi: 10.1093/nar/gkz191

Li, N., Bo, C., Zhang, Y., and Wang, L. (2021). PHYTOCHROME INTERACTING FACTORS PIF4 and PIF5 promote heat stress induced leaf senescence in Arabidopsis. *J. Exp. Bot.* 72, 4577–4589. doi: 10.1093/jxb/erab158

Li, Y., Xi, W., Hao, J., Zhang, L., Wen, X., Wu, Z., et al. (2023). A novel tandem zinc finger protein in Gossypium hirsutum, GhTZF2, interacts with GhMORF8 to regulate cotton fiber cell development. *Agronomy* 13, 519–536. doi: 10.3390/agronomy13020519

Li, Z., Harper, J. F., Weigand, C., and Hua, J. (2023). Resting cytosol Ca2+ level maintained by Ca2+ pumps affects environmental responses in Arabidopsis. *Plant Physiol.* 191, 2534–2550. doi: 10.1093/plphys/kiad047

Lin, P. C., Pomeranz, M. C., Jikumaru, Y., Kang, S. G., Hah, C., Fujioka, S., et al. (2011). The Arabidopsis tandem zinc finger protein AtTZF1 affects ABA- and GA-mediated growth, stress and gene expression responses. *Plant J.* 65, 253–268. doi: 10.1111/j.1365-313X.2010.04419.x

Lou, L., Yu, F., Tian, M., Liu, G., Wu, Y., Wu, Y., et al. (2020). ESCRT-I component VPS23A sustains salt tolerance by strengthening the SOS module in Arabidopsis. *Mol. Plant* 13, 1134–1148. doi: 10.1016/j.molp.2020.05.010

Maldonado-Bonilla, L. D., Eschen-Lippold, L., Gago-Zachert, S., Tabassum, N., Bauer, N., Scheel, D., et al. (2014). The arabidopsis tandem zinc finger 9 protein binds RNA and mediates pathogen-associated molecular pattern-triggered immune responses. *Plant Cell Physiol.* 55, 412–425. doi: 10.1093/pcp/pct175

Motomura, K., Le, Q. T., Hamada, T., Kutsuna, N., Mano, S., Nishimura, M., et al. (2014). Diffuse decapping enzyme DCP2 accumulates in DCP1 foci under heat stress in Arabidopsis thaliana. *Plant Cell Physiol.* 56, 107–115. doi: 10.1093/pcp/pcu151

Pomeranz, M. C., Hah, C., Lin, P. C., Kang, S. G., Finer, J. J., Blackshear, P. J., et al. (2010). The Arabidopsis tandem zinc finger protein AtTZF1 traffics between the nucleus and cytoplasmic foci and binds both DNA and RNA. *Plant Physiol.* 152, 151–165. doi: 10.1104/pp.109.145656

Qu, J., Kang, S. G., Wang, W., Musier-Forsyth, K., and Jang, J. C. (2014). The Arabidopsis thaliana tandem zinc finger 1 (AtTZF1) protein in RNA binding and decay. *Plant J.* 78, 452–467. doi: 10.1111/tpj.12485

Ripin, N., and Parker, R. (2023). Formation, function, and pathology of RNP granules. *Cell* 186, 4737–4756. doi: 10.1016/j.cell.2023.09.006

Sheen, J. (2001). Signal transduction in maize and Arabidopsis mesophyll protoplasts. *Plant Physiol.* 127, 1466–1475. doi: 10.1104/pp.010820

Shi, H., Liu, W., Wei, Y., and Ye, T. (2017). Integration of auxin/indole-3-acetic acid 17 and RGA-LIKE3 confers salt stress resistance through stabilization by nitric oxide in Arabidopsis. *J. Exp. Bot.* 68, 1239–1249. doi: 10.1093/jxb/erw508

Solis-Miranda, J., Chodasiewicz, M., Skirycz, A., Fernie, A. R., Moschou, P. N., Bozhkov, P. V., et al. (2023). Stress-related biomolecular condensates in plants. *Plant Cell* 35, 3187–3204. doi: 10.1093/plcell/koad127

Song, H., Zhao, R., Fan, P., Wang, X., Chen, X., and Li, Y. (2009). Overexpression of AtHsp90.2, AtHsp90.5 and AtHsp90.7 in Arabidopsis thaliana enhances plant sensitivity to salt and drought stresses. *Planta* 229, 955–964. doi: 10.1007/s00425-008-0886-y

Sorenson, R., and Bailey-Serres, J. (2014). Selective mRNA sequestration by OLIGOURIDYLATE-BINDING PROTEIN 1 contributes to translational control during hypoxia in Arabidopsis. *Proc. Natl. Acad. Sci. U.S.A.* 111, 2373–2378. doi: 10.1073/pnas.1314851111

Sun, J., Jiang, H., Xu, Y., Li, H., Wu, X., Xie, Q., et al. (2007). The CCCH-type zinc finger proteins AtSZF1 and AtSZF2 regulate salt stress responses in Arabidopsis. *Plant Cell Physiol.* 48, 1148–1158. doi: 10.1093/pcp/pcm088

Sun, Y., Kong, X., Li, C., Liu, Y., and Ding, Z. (2015). Potassium Retention under Salt Stress Is Associated with Natural Variation in Salinity Tolerance among Arabidopsis Accessions. *PloS One* 10, e0124032. doi: 10.1371/journal.pone.0124032

Xu, J., Huang, Z., Du, H., Tang, M., Fan, P., Yu, J., et al. (2023). SEC1-C3H39 module fine-tunes cold tolerance by mediating its target mRNA degradation in tomato. *New Phytol.* 237, 870–884. doi: 10.1111/nph.18568

Yang, Y., and Guo, Y. (2018). Elucidating the molecular mechanisms mediating plant salt-stress responses. *New Phytol.* 217, 523–539. doi: 10.1111/nph.14920

Yin, X., Xia, Y., Xie, Q., Cao, Y., Wang, Z., Hao, G., et al. (2020). The protein kinase complex CBL10-CIPK8-SOS1 functions in Arabidopsis to regulate salt tolerance. *J. Exp. Bot.* 71, 1801–1814. doi: 10.1093/jxb/erz549

Zeng, Y., Li, Q., Wang, H., Zhang, J., Du, J., Feng, H., et al. (2018). Two NHX-type transporters from Helianthus tuberosus improve the tolerance of rice to salinity and nutrient deficiency stress. *Plant Biotechnol. J.* 16, 310–321. doi: 10.1111/pbi.12773

Zhang, H. X., and Blumwald, E. (2001). Transgenic salt-tolerant tomato plants accumulate salt in foliage but not in fruit. *Nat. Biotechnol.* 19, 765–768. doi: 10.1038/90824

Zhao, S., Zhang, Q., Liu, M., Zhou, H., Ma, C., and Wang, P. (2021). Regulation of plant responses to salt stress. *Int. J. Mol. Sci.* 22, 4609. doi: 10.3390/ijms22094609

Zhu, J. K. (2002). Salt and drought stress signal transduction in plants. *Annu. Rev. Plant Biol.* 53, 247–273. doi: 10.1146/annurev.arplant.53.091401.143329

Zhu, J. K. (2016). Abiotic stress signaling and responses in plants. *Cell* 167, 313–324. doi: 10.1016/j.cell.2016.08.029